

I

Introduction

1

Modern Trends in Advanced Ceramics

Ralf Riedel, Emanuel Ionescu, and I.-Wei Chen

1.1

Advanced Ceramics

Ceramics are defined as inorganic, non-metallic materials which are typically crystalline in nature and contain metallic and non-metallic elements such as Al_2O_3 , CaO , ZrO_2 , SiC , and Si_3N_4 . There are several broad categories of ceramics classifying the industrial products as follows: clay products, white ware, refractories, glasses, cements, abrasives, and advanced ceramics.

Advanced ceramics are materials tailored to possess exceptional properties (superior mechanical properties, corrosion/oxidation resistance, thermal, electrical, optical or magnetic properties) by controlling their composition and internal structure. They are subdivided into *structural ceramics* (wear parts, cutting tools, engine components and bioceramics), *electrical ceramics* (capacitors, insulators, substrates, integrated circuit packages, piezoelectrics, magnets and superconductors), *ceramic coatings* (engine components, cutting tools and industrial wear parts) and *chemical processing* and *environmental ceramics* (filters, membranes, catalysts and catalyst supports).

As an example of advanced ceramics, silicon carbide (SiC) bearings for chemical plants are shown in Figure 1.1. This type of device must withstand aggressive chemical environments, show high compressive strength, high stiffness, low density, high fracture resistance, and remain stable under thermal stress.

1.2

Conventional Synthesis and Processing of Advanced Ceramics

1.2.1

Synthesis of Ceramic Powders

The preparation of ceramic products typically involves heating processes of ceramic powders which must undergo special handling in order to control purity, particle

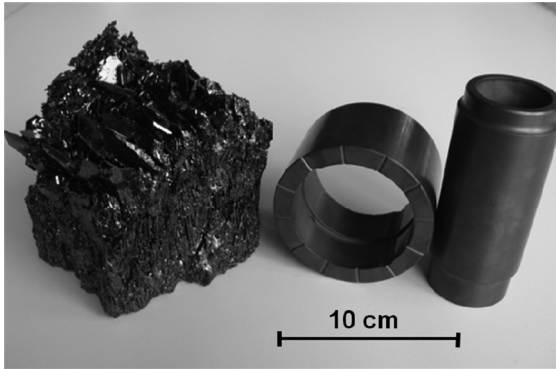


Figure 1.1 High-temperature and corrosion-resistant silicon carbide (SiC) advanced ceramic (right) produced from silicon carbide raw material (left) obtained by the reaction of silica with carbon at temperature $>2000^{\circ}\text{C}$, according to the Acheson process.

size, particle size distribution, and heterogeneity. These factors play an important role in the properties of the finished ceramic part. In principle, it is possible to distinguish finished ceramics made of naturally harvested materials from fully synthetically prepared starting materials. While most of the binary oxide ceramics such as alumina or silica can be processed from natural sources, non-oxide ceramics and more complex oxides such as high-temperature superconductors must be obtained by complex synthetic routes. Both the natural products and the synthetic materials must be controlled in terms of their chemical compositions and homogeneity, specific shape, particle size, and particle size distribution (Figure 1.2).

There are several synthetic methods for the preparation of ceramic powders. *Solid-state reactions* are the most widely used processes as they are suitable for the

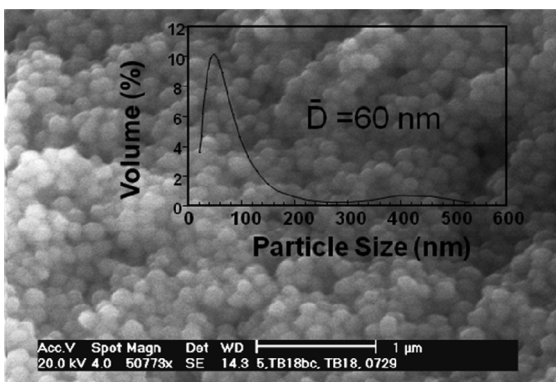


Figure 1.2 SEM image of a sol-gel-derived silicon carbide/nitride-based composite powder. The particle size distribution of the powder is shown in the inset.

mass-production of cost-efficient powders. Highly pure ultrafine powders are synthesized via *gas-phase reactions*. *Liquid-phase synthesis* for producing homogeneous fine ceramic powders involves the co-precipitation method and a hydrothermal synthesis. In most synthesis routes, temperature is the main reaction-controlling parameter. In recent approaches related to the search for new synthetic compounds, pressure has been used in addition to temperature for the synthesis of novel nitrides such as γ - Si_3N_4 or cubic Hf_3N_4 and Zr_3N_4 . Laser-heated diamond anvil cell and multi anvil techniques have been successfully applied for basic high-pressure ceramic synthesis studies (Figures 1.3 and 1.4) [1,2].

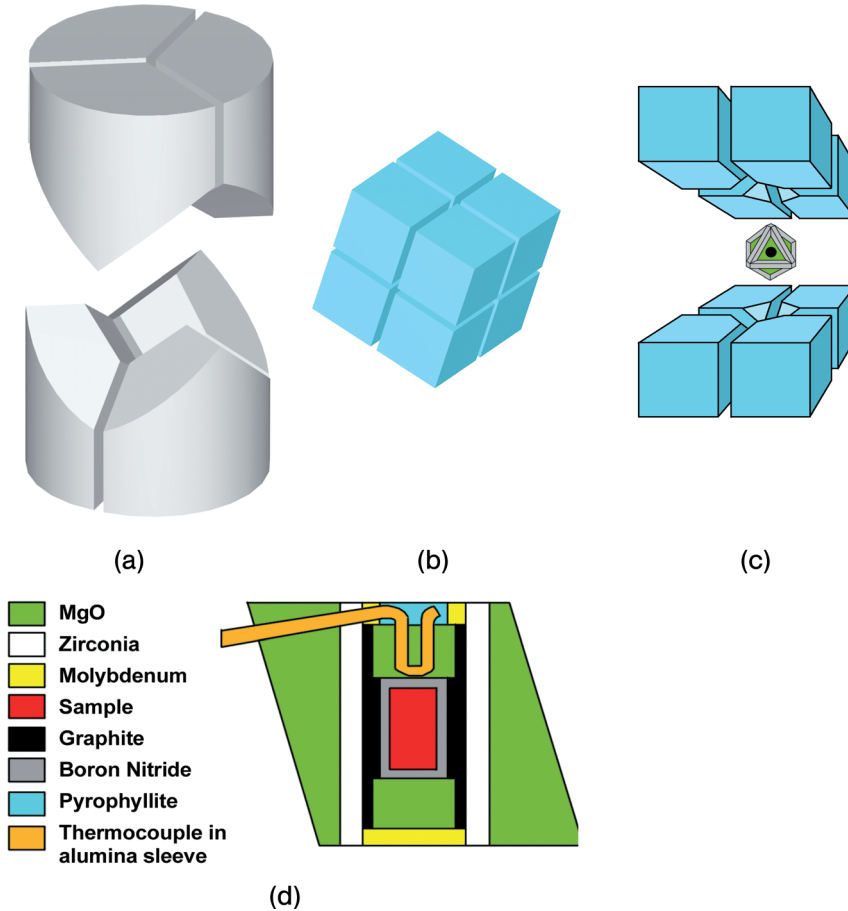


Figure 1.3 Schematic drawing of a multi anvil (MA) apparatus for high-pressure/high-temperature materials synthesis. (a) Walker-type module. (b) Eight tungsten carbide cubic anvils. (c) Schematics of compression of the octahedral pressure cell between eight truncated tungsten carbide anvils. (d) Cross-section of the octahedral pressure cell. The MA cell can be operated up to 25 GPa pressure and up to 2400 °C.

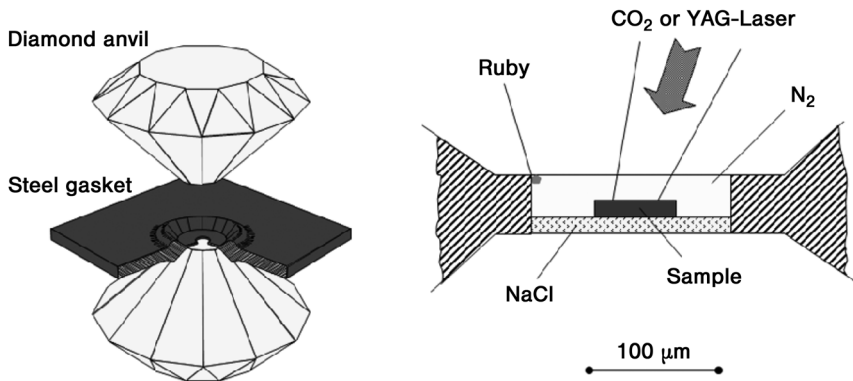


Figure 1.4 Schematic drawing of a laser-heated diamond anvil cell (LH-DAC) for the high-pressure and high-temperature materials synthesis (left). The inset on the right shows the sample holder device. The LH-DAC can be operated at pressures up to 100 GPa and 7000 °C. For further details, see Refs. [1,2].

1.2.2

Forming

Forming processes involve a mix, slip, or plastic material which is formed into a shape. It is generally desirable to have high green densities, as this factor acts against the firing shrinkage. This leads also to reduced rejects and lower firing temperatures.

There are several forming processes for advanced ceramics. Some of these are classified as traditional, namely die pressing or cold isostatic pressing (CIP). Slip casting and extrusion, tape casting and injection-molding processes are classified as wet and high-tech forming processes.

Die pressing is by far the most frequently used forming process for advanced ceramics, and involves the uniaxial compaction of a granulated powder during confined compression in a die. The pressed green bodies can be then fired directly or after isostatic pressing.

Isostatic pressing involves the shaping of granular powders in a flexible, air-tight container placed in a closed vessel filled with pressurized liquid. This method assures a uniform compaction of the powders into a green body that retains the general shape of the flexible container and any internal tooling profile.

Slip casting of ceramics is a technique that has long been used for manufacturing traditional ceramics. The advantages of slip casting include its ability to form green bodies of a complex shape, without expensive tooling. The bodies produced are almost invariably thin-walled with a uniform thickness. It is an inexpensive process when compared with other ceramic manufacturing techniques. A slip is prepared by ball-milling the appropriate powders along with binders, plasticizers, deflocculants, etc., in a solvent or water. In order to reproduce the castings, it is essential that the

slip is characterized by means of its viscosity, dilatancy, solids content, etc. Such a slip is poured into a porous mold, where the liquid part of the slip will be absorbed by capillary action into the mold to leave a layer of ceramic and additives formed against the plaster. It is possible to improve green density and impart higher green strength on a cast body by applying an ultrasonic frequency to the mold during casting. Another way to improve green body characteristics is to apply pressure (e.g., by gas) to the slip during casting. This can yield higher densities and minimize shrinkage after casting.

Due to the poor ductility and the high flow stress of ceramics, *extrusion process* should be performed under a higher temperature and slower speed than for the metals in order to reduce the flow stress and to avoid fracture. *Hot extrusion* can be a promising ceramic manufacturing technique if a textured structure is desired. Nevertheless, this method is limited to large cross-section products of non-structural ceramics with a low melting point [3].

Tape casting is used for producing, for example, multilayered capacitors, multilayered ceramic packages, piezoelectrics, ceramic fuel cells, and lithium ion batteries. The advantage of the tape casting method is that it is the best technique for creating large, thin and flat ceramic parts, which are impossible to produce with other techniques such as pressing or extrusion. In the ceramic industries, the process of tape casting is considered comparable to traditional slip casting as it also uses a fluid suspension of ceramic particles as the starting point for processing.

Injection-molding is a suitable process for the high-volume production of complex design parts, and for manufacturing complex precision components with the highest degree of repeatability and reproducibility. It is a combination of powder, injection-molding and sintering technologies. The injection-molding process has the advantage that it is a near net shape technique, so that grinding or major external finishing of the produced parts is not necessary.

1.2.3

Sintering

The sintering process converts the green microstructure to the microstructure of the dense ceramic component. In this way, sintering is the last of the ceramic processing steps where the ceramist has an influence on microstructural development. This influence is limited, however, as the worst inhomogeneities that pre-exist in the compact are usually exaggerated during sintering; for example, flaws will persist or even grow, while large particles may induce abnormal grain growth.

The sintering process consists of solid particle bonding or neck formation, followed by continuous closing of pores from a large open porosity to essentially pore-free bodies. There are various sintering processes which occur by different mechanisms. Traditional household and sanitary ceramic ware are densified by viscous flow. In contrast, technical or advanced ceramics are produced by liquid-phase and solid-phase sintering, which utilize significantly smaller amounts of sintering additives as compared to viscous flow densification. *Liquid-phase sintering* involves solution–reprecipitation and diffusion mechanisms, while *solid-state sintering* is dominated

by volume and grain boundary diffusion mechanisms responding to free energy and chemical potential differences. Another method of producing advanced ceramics is the *reactive sintering* processes. Here, the solid phase precipitates from an intermediary liquid phase which is generated during compaction. In a recent review, the phenomena associated with sintering have been fundamentally discussed from a theoretical point of view [4].

When the particle size of the precursor powders decreases to nanosized powders, new mechanisms such as grain boundary slip, dislocation motion, grain rotation, viscous flow and grain boundary melting become operative. Furthermore, sintering of nanopowders enjoys a high driving force and enhanced kinetics due to the curvature effect. Thus, the densification of nanopowders occurs at temperatures significantly below those of larger-grained powders by up to several hundreds of degrees. Consequently, small final grain sizes may result and sintering aids and undesirable phase transformation may be avoided.

For the enhanced densification of ceramic powders, pressure-assisted consolidation methods such as hot pressing, hot isostatic pressing, sinter forging, hot extrusion or ultra-high pressure sintering can be applied. *Hot pressing* is a technique which combines external uniaxial pressure with temperature in order to enhance densification. Hot pressing is only suited to relatively simple shapes, with the products usually requiring subsequent diamond grinding to achieve the finished tolerances. The *hot isostatic pressing* (HIP) technique combines high temperature and a gas pressure, which is uniformly applied to the powders in all directions. This is used industrially to produce defect-free castings, complex shaped components, or high-density ceramics and composites. As the interface must be isolated from the gaseous pressure medium, encapsulation of the component is often performed. In order to transmit the gas pressure to the powder compact or previously partially sintered part, a gas-impermeable membrane which encapsulates the compact or part must be provided. This can be achieved either by sealing of the exterior surface of the compact or partially sintered part, or by placing a flexible sleeve around them. A partially sintered body containing no open porosity can, however, be hot-isostatically pressed directly.

Besides these methods, a number of non-conventional consolidation techniques have been applied to ceramic powder sintering, including *microwave sintering*, *shock* or *dynamic consolidation* and *field assisted sintering*.

Microwave sintering is characterized by reduced temperature gradients and processing times due to the direct energy coupling with electric dipoles within the heating body [5]. The reduced processing time brings final property benefits by reducing the grain growth. This is, in part, achieved by bypassing the low-temperature region where the rate of grain growth is higher than the rate of densification.

Shock or *dynamic consolidation* occurs by the passage of a large-amplitude compressive stress generated by plate impact or explosion, whereby no external heating is applied. Thus, densification proceeds by plastic yielding; high temperatures (up to melting temperatures) due to particle interfriction enable good interparticle bonding. Whereas in coarse materials the heating is only superficial, in nanopowders the heat may transfer throughout the entire particle, thus retaining the fine grain size or out-of-equilibrium conditions (amorphous structures [6], supersaturated solid solutions [7]).

One major drawback of this method is the difficult coordination of the short stress waves and heat generation events, which frequently leave specimens fractured.

Spark plasma sintering (SPS) is a field-assisted compaction method which allows very rapid heating and cooling rates, very short holding times, and the preparation of fully dense samples at comparatively low sintering temperatures, typically a few hundred degrees lower than in normal hot sintering. Instead of using an external heat source (as in conventional hot pressing), an electrical current (DC, pulsed DC, or AC) is allowed to pass through the conducting pressure die and, in some cases, also through the sample; in this way the die itself acts as a heat source, so the sample is heated from both inside and outside. In the SPS process, a pulsed DC (typically 3.3 ms of 0.5 to 10 kA intensity) is applied for the whole time period of the sintering cycle. The SPS process allows the possibility of using very rapid heating rates (up to $600\text{ }^{\circ}\text{C min}^{-1}$ or more) and very short holding times (minutes) to obtain fully dense samples at comparatively low sintering temperatures. The factors that contribute to the rapid densification process are: a mechanical pressure exceeding that used in normal hot pressing processes; fast heating and cooling rates; and the exposure to an electric field [8]. The spark plasma sintering method has found applications in the preparation of dense compacts containing nanosized grains (such as ZnO, Al_2O_3) [5,9], metastable constituents (e.g., α -sialons, $\text{M}_x\text{Si}_{12-(m+n)}\text{Al}_{m+n}\text{O}_n\text{N}_{16-n}$, $\text{M}=\text{Ce}$, La, Sr, Eu, Ba) [10], and laminated structures of dissimilar ceramics ($\text{TiN}/\text{Al}_2\text{O}_3$, $(\text{TiN})_x(\text{Al}_2\text{O}_3)_{1-x}$) [11]. Other field-assisted sintering methods are *plasma-activated sintering* (PSA), *field-activated sintering technique* (FAST) or *pulse electro-discharge consolidation* which have been effectively applied to nanopowder consolidation [12].

After sintering, the consolidated and densified ceramic body is characterized by its typical microstructure. The microstructure developed during sintering is determined not only by the composition of the starting powder but also by the method of sintering and by the applied gases, pressure, time and temperature. Figure 1.5

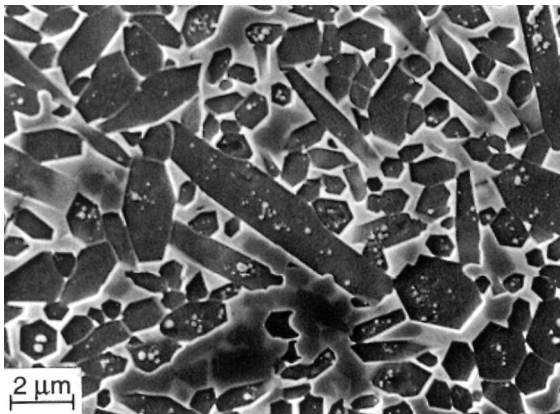


Figure 1.5 SEM image of a dense $\text{Si}_3\text{N}_4/\text{SiC}$ micro/nano-composite ceramic obtained by liquid-phase sintering of amorphous SiCN powder.

represents a typical microstructure comprising of Si_3N_4 and SiC obtained by liquid-phase sintering of a polysilazane-derived amorphous SiCN composite powder. The microstructure can be described as a nano/micro composite with nanosized β -SiC grains and micron sized β - Si_3N_4 crystallites [13].

1.2.4

Finishing

Every ceramic component in its *as-processed* state has individual features due to uncontrollable minor changes in processing. Due to differential shrinkage and gravity effects during sintering, these can accumulate to a minimum of 1–2% distortion. This is in contrast to similar metallic or polymeric components, which maintain in-processing dimensional stability within a fraction of 1%. Thus, machining is usually required in order to bring advanced ceramic components to a common standard. Routine machining of metal components to 25 μm tolerance (1/1000-in) poses no difficulty or exaggerated costs, while similar tolerances for ceramics require expensive precision diamond grinding. Distortion in the green forming and sintering of ceramics is typically $\pm 2\%$ of the linear average dimensions. Unless post-sintering diamond machining is performed, the $\pm 2\%$ tolerance is typical for ceramic components. For very small parts, the relative (percentage) tolerance usually increases, and frequently the tolerances of as-fired ceramics are 2% or 0.2 mm, whichever is greater. Diamond-machined (ground) components have typical tolerances of 20 μm . Much better tolerances ($\sim 1 \mu\text{m}$) are achievable for lapped and polished components.

Machining is the controlled destruction of the surface to produce the desired shape, size, finish, and strength. Machining of sintered ceramics should be undertaken only when it is not possible to achieve the necessary dimensional tolerance by other techniques, such as optimization of forming and sintering to avoid deformation, minimization of densification shrinkage (e.g., through reaction bonding of Si_3N_4 , SiC, Al_2O_3), and green (before sintering) or white (after a pre-sintering step) machining. When needed, the machining costs of sintered ceramics are very high: even performing the relatively simple machining of a ceramic cutting tool incurs a cost that is approximately 60–80% of the total manufacturing costs.

Only a limited number of processes exist for finishing fully sintered advanced ceramics, such as grinding, lapping, polishing (which can be done with cutting tools having geometrically undefined cutting edges), and turning, drilling or milling (where the cutting tools have geometrically defined cutting edges) [14]. Naturally, the cutting tool materials are very hard; for example, polycrystalline diamond (PCD) or cubic boron nitride (CBN) are often used.

Grinding is an abrasive process that involves abrasive grits (hard particles with sharp edges) bonded into a wheel which rotates at a high speed. The orientation of the individual grains is random; thus, a grain may encounter the working surface with a positive, zero, or negative rake angle. The geometry of grinding is variable, including surface grinding with a horizontal or vertical spindle, cylindrical grinding, internal grinding, centerless grinding, and form (plunge) grinding [15].

Honing is a technology for the mechanical finishing of brittle-hard ceramics and metallic parts that renders the smoothest surface texture and the greatest accuracy. It is defined as cutting with geometrically undefined cutting edges, during which multi-edge tools show a motion consisting of two components: the stroke motion, so that the machined surface shows defined crossing traces; and a rotary motion. There are many variants of honing, such as plane, round, screw, profile, and form honing (*long-stroke honing*) and superfinishing (*short-stroke honing*). Long-stroke honing allows a high surface quality and makes possible the smooth finish of internal cylindrical surfaces with a high dimensional and form accuracy. The short-stroke honing (superfinishing) technology finds applications in machining friction and sliding surfaces, parts of antifriction bearings and slide bearing pivots, as well as sliders and seats of packing rings and collars [11].

Lapping and *polishing* are machining techniques with loose abrasives, and function by the sliding frictions between particles and a surface. The lap or polisher travels across a work surface against which particles of sand or mud-type slurry are forced to the point of contact. The work piece shows a planetary movement and acquires a uniformly-machined, random, flat finish.

Due to the high machining cost of advanced ceramics, several *near-net-shape technologies* were developed in order to produce complex-shaped components with a minimal need for machining. Near-net-shape processes involve the optimization and control of each production process step, thus minimizing the number and size of microstructural defects to within design limits [16]. For instance, *injection-molding* is a suitable method for near-net-shape production of ceramic parts, requiring little subsequent grinding and no need for machining. Ceramic injection-molding allows the production of a wide range of component sizes and shapes for various ceramic materials [17]. Colloidal forming methods (such as clay-like forming [18], direct coagulation casting (DCC) [19], gel casting [20], and hydrolysis-assisted solidification (HAS) [21] for consolidating ceramic slurries into uniform, defect-free powder compacts have been also proved to be suitable for producing near-net-shape components.

During the past few years, several more new near-net-shape methods have been developed, such as *solid freeform fabrication* (SFF) or *temperature-induced forming* (TIF). The SFF method allows the mold-free manufacture of ceramics by adding materials layer by layer. Current SFF techniques include laminated object manufacturing (LOM) [22], selective laser sintering (SLS) [23], stereolithography (SL) [24], fused deposition of ceramics (FDC) [25], 3-D-printing [26], and direct-inkjet printing (DIP) [27]. In the TIF technique, the consolidation of a highly filled ceramic slurry is achieved simply by increasing the temperature. As no dispersing media need to be removed, non-porous molds can be used for shaping [12].

1.3

Molecular Routes for the Synthesis and Processing of Advanced Ceramics

In addition to the traditional powder manufacturing processes, more recently methods such as chemical vapor deposition (CVD), the sol-gel technique and polymer

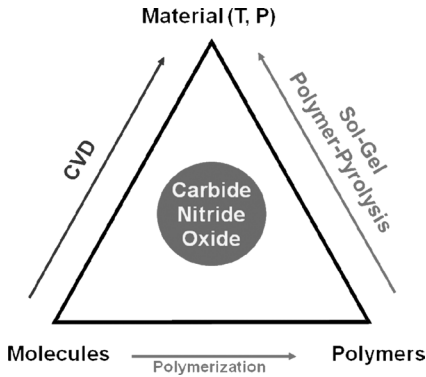


Figure 1.6 Molecular materials synthesis can be achieved via chemical vapor deposition (CVD), polymer pyrolysis, or sol–gel techniques. In the latter cases, the so-called “bottom up” approach requires that the molecules must be transformed to polymers before transformation to the desired inorganic material. P, pressure; T, temperature.

pyrolysis have been applied to create high-purity starting materials with defined properties. Furthermore, these processes can open up new areas of application previously unrealizable by conventional methods. In all three processes, the ceramic solid is synthesized on the basis of lower molecular, inorganic or elemental organic precursors (Figure 1.6).

The aim of present research activities in the materials synthesis field is to develop concepts for the production of novel multifunctional inorganic materials with a tailor-made, nanoscaled structure. Industrial demands on future technologies have created a need for new material properties which exceed by far those of materials known today, and which can only be produced by designing the material structure at a nanoscale. Furthermore, the increasing miniaturization of components calls for new process technologies which allow the reliable production of materials at and below a micrometer scale. In particular, inorganic–organic hybrid materials as well as amorphous and polycrystalline ceramics are to be used as material classes and produced by means of crosslinking routes in various states of condensation. In accordance with the so-called “bottom-up” approach, specific inorganic molecules are to be assigned to higher molecular networks and solid-state structures in the form of molecular nanotools by means of condensation and polymerization processes. This method aims at linking organic components to inorganic structures, thus producing materials inaccessible by thermodynamically controlled chemical syntheses. Therefore, experimental studies focus on the development of solids derived from molecular units via kinetically controlled synthesis processes in the interface between molecular and solid-state chemistry enabling specific adjustments to be made to the solid-state properties. Thus, the ultimate objective of the present-day investigations in this field is to systematically to study the “bottom-up” approach with regard to the synthesis and exploration of novel materials. In this way it should

be possible to establish the technological fundamentals for the development of these new materials and their potential use. Possible fields of application for materials produced at a nanoscale are key technologies of the 21st century such as transport systems, information technology and energy, as well as environmental systems and micro- or nano-electromechanical systems. The correlation between the structure of the molecular precursors and the nanostructure of the derived materials and their properties will provide the focal point for detailed experimental studies.

In the following sections, the molecular routes which have great potential for use in ceramic manufacturing and processing are briefly described.

1.3.1

The CVD Process

In the CVD process, lower molecular, volatile reactants in the gas phase are fed into a hot reaction zone in which a solid reaction product results, which may be collected either as a free powder or as a coating on a substrate. The deposition temperatures for ceramic products range from 600 to 1500 °C, depending on the reaction system [28,29]. If a plasma or laser is utilized to enhance the chemical reaction rate of the precursors, the formation of the ceramic product can be effected at temperatures below 500 °C. Some reaction systems and their ceramic products are detailed in Table 1.1. The thermodynamic instability of the gaseous reactants provides the driving force for the reaction. The total deposition rate depends on the reaction rate, nucleation rate, and diffusion rate. The rate-determining factor at higher temperatures is diffusion, whereas at lower temperatures it is reaction.

The CVD process is primarily used for:

- gas-phase infiltration of porous substrates [30]
- coatings and surface modification [24,31]
- production of ceramic whiskers
- high-purity, fine ceramic powders [32]

Figure 1.7 shows a hard, amorphous coating comprised of SiCN derived by plasma-enhanced CVD using a molecular precursor, namely $R_3Si-N=C=N-SiR_3$

Table 1.1 Reaction systems for chemical vapor deposition (CVD) of ceramic compounds.

Reaction system ^a	Temperature [°C]	Ceramic product	Process
AlCl ₃ /NH ₃	800–1200	AlN	CVD
AlCl ₃ /NH ₃	400–600	AlN	PACVD ^b
BCl ₃ /NH ₃	800–1200	BN	CVD
Si(CH ₃) ₄	900–1400	SiC	CVD
Si(Cl ₄)/NH ₃	1000–1400	Si ₃ N ₄	CVD
SiCl ₄ /NH ₃	400–600	Si ₃ N ₄	PACVD ^b

^aData from Refs. [28] and [29].

^bPlasma-assisted CVD.

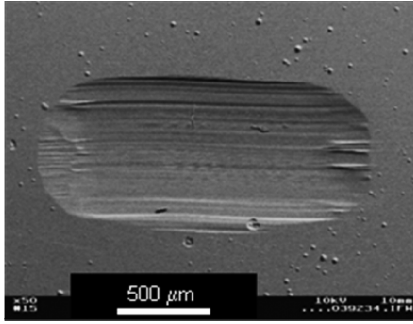


Figure 1.7 SEM image of a wear track of an amorphous SiCN hard coating on a steel substrate. The coating was produced by a radiofrequency plasma-enhanced chemical vapor deposition process (RF PE-CVD) using $R_3Si-N=C=N-SiR_3$ ($R=CH_3$) as molecular single source precursor. The achieved film thickness is in the order of $20\ \mu\text{m}$, and the hardness was determined as being in the range 21–29 GPa. For more details, see Ref. [33].

with $R=CH_3$, having all required elements silicon, carbon and nitrogen in the molecular structure [33].

In general, the CVD reaction system may be described by Eq. (1)



in which A mole of gas a and B mole of gas b react to C mole of solid phase c (ceramic) and D mole of gaseous reaction product d. The appropriate reaction conditions may be specified as the partial pressures of all the gases and the temperature.

The formation of free ceramic powders in the reactor atmosphere results from homogeneous nucleation. In contrast, deposition of substrate films or whiskers proceeds by heterogeneous nucleation. Homogeneous nucleation requires a higher supersaturation S of the gas phase [29] which is dependent on the equilibrium constant K of the reaction system [Eq. (2)] and the partial pressures of the reactant and product gases:

$$S = \frac{[a]^A [b]^B}{[d]^D} K \quad (2)$$

The equilibrium constant itself is strongly temperature-dependent, as exemplified by thermodynamic calculations in the system $AlCl_3/NH_3$ [32]. The values of K in the temperature range between 1000 and 1500 °C calculated from the JANAF tables are listed in Table 1.2 [34]. Due to the temperature dependence of K in accordance with Eq. (2), it can be predicted – and confirmed experimentally – that high temperatures favor the formation of AlN powders, while low temperatures favor the formation of a AlN substrate film [32].

Table 1.2 Temperature-dependent thermodynamic data of the reaction system $\text{AlCl}_3/\text{NH}_3$.

$\text{AlCl}_{3(\text{g})} + \text{NH}_{3(\text{g})} \rightleftharpoons \text{AlN}_{(\text{s})} + 3\text{HCl}_{(\text{g})}$		
Temperature [°C]	$\Delta G \frac{T}{R}$ [kJ mol ⁻¹]	ln K_p
800	-48.4	5.4
1000	-65.2	6.2
1200	-82.0	6.7
1400	-99.0	7.1
1500	-107.5	7.3

In gas-phase infiltration, it is essential to operate at lower temperatures in order to avoid powder formation. To avoid long diffusion routes of reaction gases in porous materials, the maximum infiltration depth is low, for example 4.5 mm for deposition of SiC in porous graphite with a defined pore radius of 20 μm and a reaction temperature of 900 °C [30].

1.3.2

The Sol–Gel Process

The sol–gel process involves the manufacturing of oxide ceramics via hydrolysis of metal salts or peptization of metal oxides with subsequent coagulation of the product colloids (colloidal gels). Alternatively, it may involve the hydrolysis of alcoholic solutions of metal alkoxides, formates, acetates or acetylacetonates forming polymeric gels.

The formation of colloidal gels is preceded by the formation of a sol (particle size 0.01–0.1 μm), whereby the suspended colloidal particles are in either electrostatic (pH) or steric interaction by means of surface-active or polymer substances. Upon destabilization of the sols – for example, by changing the pH value or by removing the liquid phase – the sol particles coagulate and form a 3-D gel. Unlike the polymer gels, the formation of colloidal gels is reversible.



The hydrolysis of metal alkoxides dissolved in alcohol leads to condensation reactions and the ensuing formation of inorganic polymers with M–O–M as a structural unit; this reaction is driven towards completion by removal of the product water. Both linear and crosslinked polymers can result from partial hydrolysis, depending on the stoichiometric ratio of water and alkoxide, and the concentration of the added acid or base catalyst. Progressive poly-condensation gradually leads to gel formation. In the next step, the wet gel is transformed to a xerogel by the extraction of the solvent (drying process). The conversion of the M–O–M-containing polymer or gel into metal oxide (which can be considered as a macromolecule) is

accomplished via heat treatment in several calcination steps entailing the following reactions subject to the temperature:

- 100–200 °C: separation of adsorbed solvent particles (water, alcohol)
- 200–600 °C: decomposition of organic residues and hydroxide, nitrate, sulfate, etc.
- 100–700 °C: inter- and intramolecular separation of water and alcohol forming the corresponding metal oxide.

As demonstrated in detailed investigations on the hydrolysis of tetraethoxy silane, the complete hydrolysis of alkoxides provides sol particles which aggregate to form a colloidal gel according to the pH value or dilution [35]. Some examples of oxide materials produced by hydrolysis of metal alkoxides via this process are listed in Table 1.3.

The drying process plays a decisive role in the production of defect-free gels – that is, dense, crack-free monolithics. During drying, considerable capillary forces come into play, and such forces increase with decreasing capillary radius according to the Laplace equation [36,37]:

$$\Delta P = 2\gamma\cos\Theta/r_p \quad (4)$$

Here r_p is the capillary radius, γ is the surface energy of the liquid, and Θ is the contact angle at the gel–liquid–air interface. The capillaries may collapse upon crack formation, as discussed in detail by Scherer [37] or Defay [36].

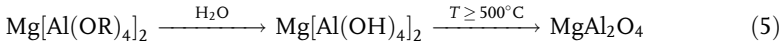
In order to avoid crack formation, the gel must be dried at an extremely slow rate under controlled vapor pressure of the solvent. As the drying rate is inversely proportional to the sample thickness, the crack-free drying process may take several weeks. After overcoming these initial difficulties, it was nevertheless possible to create ceramic products with larger dimensions directly from alkoxides. Thus, high-purity glass panes for optical applications could be obtained [45].

An understanding of the hydrolysis kinetics of the individual metal compounds plays a decisive role in the hydrolysis of alkoxide mixtures for the production of multiphase ceramics. Double alkoxides such as $\text{Mg}[\text{Al}(\text{OR})_4]_2$ with $\text{R}=\text{Alkyl}$ [44] are

Table 1.3 Metal alkoxides for the production of oxidic ceramics.

Metal alkoxide	Ceramic
$\text{Ba}(\text{OEt})_2$	BaO [38]
$\text{Y}(\text{OPr})_3$	Y_2O_3 [39]
$\text{Al}(\text{OEt})_3$	Al_2O_3 [40]
$\text{Si}(\text{OEt})_4$	SiO_2 [41]
$\text{Ti}(\text{OEt})_4$	TiO_2 [42]
$\text{Zr}(\text{OEt})_4$	ZrO_2 [43]
$\text{Mg}[\text{Al}(\text{OEt})_4]_2$	MgAl_2O_4 [44]

present in the solution as molecular species, and therefore exhibit uniform reaction kinetics in the hydrolysis process:



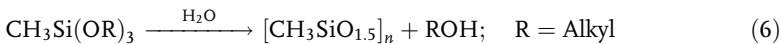
Therefore, starting from $\text{Mg}[\text{Al}(\text{OR})_4]_2$ it is possible to manufacture a phase-pure spinel, for example a spinel membrane, via the sol–gel process. The membrane is applied to a microporous substrate made of $\alpha\text{-Al}_2\text{O}_3$ in the form of a crack-free film approximately 1 μm thick with an average pore radius of approximately 5 nm. Upon calcination at 1200 $^\circ\text{C}$, the deposited spinel particles exhibit crystal sizes smaller than 50 nm [46].

The Mg–Al double alkoxide was suggested by Greil *et al.* for the homogenous coating of commercial Si_3N_4 powders to provide spinel sintering additive [47]. Other metal alkoxides, such as $\text{Ti}(\text{OEt})_4$, $\text{Si}(\text{OEt})_4$ or $\text{Ba}(\text{OEt})_2$, have also been used to coat ceramic powders in order to ensure a uniform distribution of the sintering additives, directly influencing grain growth during the densification process, or to form crystalline secondary phases [48,49].

The sol–gel process may also be used to create monodisperse, submicrometer powder particles which could aid sintering because of a better packing density [50]. Thus, according to Barringer and Bowen, monodisperse Al_2O_3 can be sintered at 1250 $^\circ\text{C}$ instead of 1750 $^\circ\text{C}$, as is common in the densification of conventional Al_2O_3 powders [51]. However, since colloidal crystals still contain defects such as grain boundaries over a longer length scale, there is no significant advantage of using monodisperse powders in practical applications.

The sol–gel process is also applied for the production of oxide glass fibers and ceramic fibers [52,53], as well as for surface modification. The sol–gel coating of glass has been used in industry since the early 1970s [44]. Depending on the composition of the glass layer, it is possible to manufacture reflective or anti-reflective films [54], passive, and doped coatings (for microelectronics). Furthermore, it is also possible to produce films which, due to their low thermal expansion compared with the substrate, generate compression stress, thereby drastically increasing the mechanical strength of the glass [55]. As reported by Schubert [56,57], metal ceramic nanocomposites can be created by metal–ligand complexation bonded to silicon in the glass structure.

A further application of the sol–gel process is the production of organically modified silicates, the so-called *ormosils*. Ormosils (e.g., poly(methyl)siloxane) include non-hydrolyzable organic groups, and can be classified as inorganic–organic hybrid materials [48,51]. Their mechanical properties lie between those of pure glass and plastics.



In particular, ormosils are used to coat contact lenses, as scratch-resistant surfaces can be created [58].

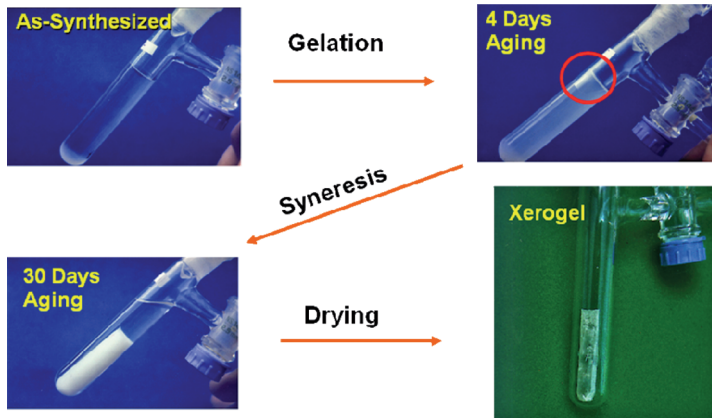
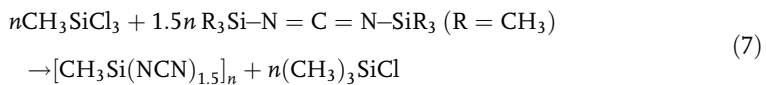


Figure 1.8 Non-aqueous sol-gel process developed for the synthesis of amorphous SiCN-gels. The gel is produced by the reaction of organochlorosilanes such as CH_3SiCl_3 , with $\text{R}_3\text{Si}-\text{N}=\text{C}=\text{N}-\text{SiR}_3$ ($\text{R}=\text{CH}_3$) in the presence of pyridine as catalyst (see Ref. [59]).

A non-aqueous sol-gel process was developed for the first time in 1997 which allowed the synthesis of nitrides and carbides by this method. A poly(methylsilyl-carbodiimide)-gel formation is shown in Figure 1.8 for the reaction of CH_3SiCl_3 with $\text{R}_3\text{Si}-\text{N}=\text{C}=\text{N}-\text{SiR}_3$ ($\text{R}=\text{CH}_3$) according to reaction Eq. (7) [59]:



A variety of other chlorosilanes as well as chlorine-substituted boron derivatives (e.g. BCl_3) or B-trichloroborazene can be reacted with $\text{R}_3\text{Si}-\text{N}=\text{C}=\text{N}-\text{SiR}_3$ to form non-oxide gels [60]. In a final step, the gels are transformed to glasses and ceramics by a thermal treatment up to 1000–1300 °C [59].

1.3.3

Polymer-Derived Ceramics (PDCs)

The production of non-oxide ceramics starting from polymeric precursors was reported for the first time during the early 1960s [61], although the first synthesis of a SiC material from polycarbosilane precursor dated back to the reports by Fritz [62] in 1956 and Yajima in 1957 [63]. Some years later, the first practical application was reported, namely the manufacture of small-diameter $\text{Si}_3\text{N}_4/\text{SiC}$ fibers from polyorganosilicon precursors for high-temperature use [64]. The Yajima process for the synthesis of SiC materials by thermolysis of polycarbosilanes was subsequently reported during the late 1970s [65].

Silicon-based polymers have proven to be promising precursors for the production of advanced ceramic components such as fibers, coatings, infiltrated porous media, or complex-shaped bulk parts. In recent years, many examples of polysilanes, polycarbosilanes, polysilazanes and polysiloxanes as precursors for ceramics have been reported [66].

Poly(organo)siloxanes are versatile materials, showing excellent chemical and physical properties. Examples of poly(organo)siloxanes are $[\text{R}_2\text{Si}-\text{O}-]_n$ or $[\text{RSi}(\text{O})_{1.5}]_n$, with $\text{R}=\text{H}$, alkyl, aryl, etc.. These have been used extensively for preparing SiCO ceramic materials via pyrolysis in inert or reactive atmospheres [67]. They have unique thermomechanical properties owing to the combination of pronounced elasticity at unusually low temperatures, and high thermal and thermo-oxidative stability at elevated temperatures. At the macroscopic level, the low-temperature elasticity of polysiloxanes is primarily manifest in some of the lowest glass transition temperatures (T_g) known for polymers, low crystalline melting points (T_m), unusually rapid crystallization, specific liquid crystalline (LC) behavior, and small viscosity-temperature coefficients [68]. Essentially, these properties are determined directly by polymer segmental chain mobilities which are all governed by the inherent chain flexibility ($\text{Si}-\text{O}-\text{Si}$ with angles from 140° to 180°) and relatively weak intra- and intermolecular interactions.

Similar to the low-temperature properties, the high-temperature stability and the degradation of polysiloxanes are also determined directly by the specific interplay of their structural building blocks – that is, the inherent strength of the siloxane bond and the pronounced flexibility of $\text{Si}-\text{O}$ segments and the whole molecule. The partial ionic and double bond character of the $\text{Si}-\text{O}$ bond in siloxanes leads to its exceptional homolytic strength, since both effects increase the binding force between the participating silicon and oxygen atoms. The reason for this was the unique additional $d_\pi-p_\pi$ bond between Si and O resulting in an $\text{Si}-\text{O}$ bond dissociation energy of about $108 \text{ kcal mol}^{-1}$, which is considerably higher than, for example, those of $\text{C}-\text{C}$ bonds ($82.6 \text{ kcal mol}^{-1}$), $\text{C}-\text{O}$ bonds ($85.2 \text{ kcal mol}^{-1}$), or even $\text{C}_{\text{arom}}-\text{C}$ bonds ($97.6 \text{ kcal mol}^{-1}$) [68]. Consequently, the $\text{Si}-\text{O}$ bond can withstand exposure to higher temperatures than the bonds normally found in organic polymers. Thus, polysiloxanes as a class exhibit higher thermal stabilities than their $\text{C}-\text{C}$ counterparts.

Silicon oxycarbide glasses can be produced only by the pyrolysis of polysiloxanes. These amorphous materials are typically black-colored due to the presence of a free carbon phase. Several studies conducted during the past few years have focused on the separation of free carbon and the microstructural development of silicon oxycarbide ceramics [69]. Furthermore, the modification of SiCO materials by boron and aluminum has attracted recent interest due to its strong influence on the thermomechanical properties and microstructure development of the silicon oxycarbide ceramics. For instance, the presence of boron in SiCO glasses inhibits the separation of free carbon, thus providing higher electrical resistivity. It has been shown via transmission electron microscopy (TEM) studies that the presence of boron induced a modified behavior in the microstructure development, in that an enhancement of finely dispersed β -SiC nanocrystallites embedded in a high-temperature stable amorphous SiBCO phase without the formation of α -cristobalite were observed for SiBCO ceramics [70]. Due

to its high temperature resistance and stable electrical properties, SiBCO is a candidate material for ceramic heaters.

Poly(organo)silazanes which contain $\equiv\text{Si}-\text{NH}-$ structural units are isoelectronic to polysiloxanes, are precursors for the production of silicon nitride and silicon carbonitride ($\text{Si}_x\text{C}_y\text{N}_z$) ceramics through high-temperature pyrolyses [71]. Although the bonding energy of the Si–O bond is higher than that of Si–N (432 and 316 kJ mol⁻¹, respectively), polysilazanes have been shown to be more thermally stable than polysiloxanes. Solid-state ²⁹Si NMR-studies have shown that polysilazane-derived Si–C–N materials are single-phase amorphous silicon carbonitride-containing SiC_xN_y ($x + y = 4$) units [72]. The insertion of boron in polysilazanes induces a dramatic enhancement of the thermal stability, and also retards crystallization up to 1800 °C. Si(B)CN ceramics can be heated to 2000 °C without degradation due to a network rearrangement which allows the amorphous Si(B)CN phase to encapsulate α -Si₃N₄ crystals, hindering the latter compound's thermal decomposition [73].

Polysilylcarbodiimides containing structural units of the form $\equiv\text{Si}-\text{N}=\text{C}=\text{N}-$ were first synthesized by Pump and Rochow via metathesis reactions of dichlorosilanes and bis(silyl)cyanamide [74]. Some three decades later, it was shown that polysilylcarbodiimides of the form $[\text{R}_2\text{Si}-\text{N}=\text{C}=\text{N}-]_n$, $[\text{RSi}(\text{N}=\text{C}=\text{N})_{1.5}]_n$, and $[\text{Si}(\text{N}=\text{C}=\text{N})_2]_n$ with R=H, alkyl or aryl, can serve as precursors for Si–C–N ceramics. Starting from polysilylcarbodiimide derivatives, the first two crystalline phases in the Si–C–N system were identified as SiC₂N₄ and Si₂CN₄ [75]. Furthermore, it was found that the synthesis of polysilylcarbodiimides starting from chlorosilanes and bis(trimethylsilyl)carbodiimide, R₃Si–N=C=N–SiR₃ (R=CH₃), in the presence of catalytic amounts of pyridine, occurs similarly to the aqueous reactions of alkoxy-silanes by means of the sol–gel process. Thus, in the non-oxide sol–gel process, bis(trimethylsilyl)carbodiimide adopts the role of H₂O, leading to Si–C–N-based gels which can be calcinated or/and pyrolyzed to Si–C–N amorphous ceramics [76].

Polysilanes and *polycarbosilanes* are classes of materials which have been subjected to a large number of investigations due to their intriguing opto-electronic properties that originate from their typical σ -conjugation [77]. For example, peralkyloligosilanes may find potential applications in photoconducting and charge-transporting materials [78]. A major factor in the interest is their use as precursors for silicon carbide materials, especially in the Yajima process for continuous SiC ceramic fibers.

In summary, silicon-containing pre-ceramic polymers provide the unique possibility for the synthesis of new ceramic systems, not only Si–C–O and Si–C–N but also Si–E–C–O (E=B, Al, Ti) and Si–E–C–N (E=B, Ti), which cannot be synthesized by means of the “classical” powder method. Since tailored properties of the final ceramic material can be achieved by chemical modification of the polymeric precursor, the PDC route offers an exceptional opportunity to synthesize novel multi-component materials with outstanding properties. These include extraordinary high-temperature and corrosion resistance, oxidation stability, and promising electric, magnetic and optoelectronic properties of interest for advanced ceramic applications [66]. Some examples of silicon-based polymers consolidated by warm pressing, and the ceramic products obtained by subsequent pyrolysis of the formed polymers, are shown in Figure 1.9.

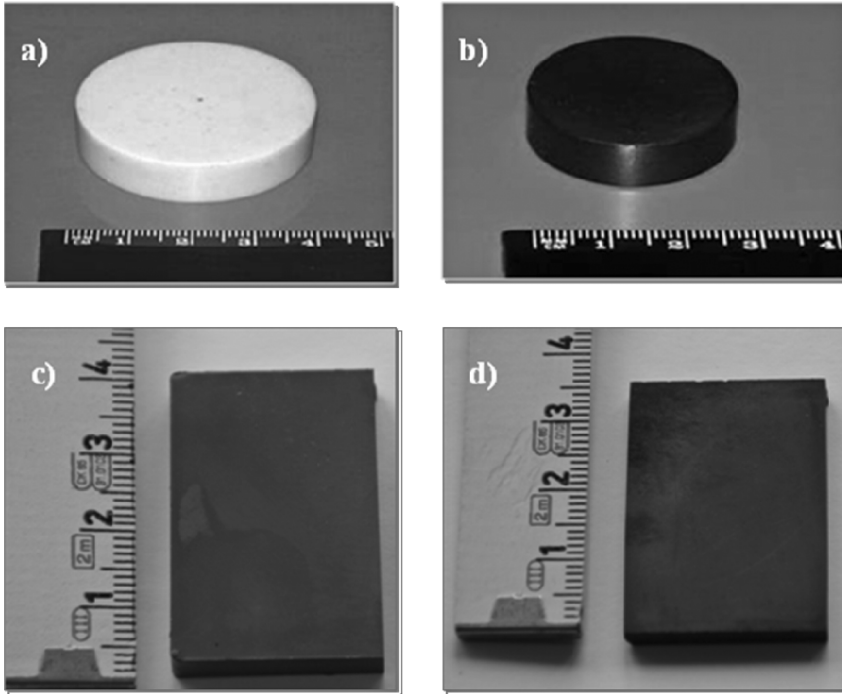


Figure 1.9 Optical micrographs of warm-pressed, silicon-based polymers and ceramic products derived therefrom by pyrolysis of the polymer at 1100 °C in Ar. (a) Crosslinked and warm-pressed polysilazane Ceraset™. (b) Amorphous SiCN

ceramic obtained by pyrolysis of sample shown in (a). (c) Crosslinked and warm-pressed polysiloxane (Wacker, MK-polymer). (d) Amorphous SiCO ceramic obtained by pyrolysis of sample shown in (c).

1.4

Methods for Characterization of Advanced Ceramic Materials

The characterization methods for advanced ceramics can be divided into optical, X-ray and electron spectroscopy techniques, resonance characterization methods, diffraction techniques, electron optical methods, and surface characterization methods. In addition, there are a variety of characterization methods which relate to the thermal and mechanical properties of ceramic materials. Some of these techniques are briefly described in the following sections.

Atomic emission spectroscopy (AES or OES) uses quantitative measurement of the optical emission from excited atoms in order to determine analyte concentrations. The analyte atoms are vaporized and atomized by a flame, discharge, or plasma. This high-temperature atomization process provides sufficient energy to promote the atoms into high energy levels. The atoms then decay back to lower levels by emitting light. As the transitions are processes between distinct atomic energy levels, the emission lines in the spectra are narrow. The major advantage of this technique (compared, for example,

with atomic absorption spectroscopy, AAS), is that all the atoms in the sample are excited simultaneously, and thus can all be detected at the same time. Various AES techniques are available, depending on the atomization source: direct current plasma (DCP); inductively coupled plasma (ICP); laser-induced breakdown excitation sources (LIBS); microwave-induced plasma (MIP); and spark and arc emission sources. The combination of electrothermal vaporization (EVT) with inductively coupled plasma atomic emission spectroscopy (ICP-AES) was shown to be a promising method for the analysis of ceramic powders [79]. Since carbide-forming elements in powdered ceramic materials are difficult to vaporize, several studies were conducted on chemical modifiers. Substances such as KF, $(C_2F_4)_n$, $Na_2B_4O_7$, $BaCO_3$, $Ba(NO_3)_2$, BaO, AgCl, CoF_2 and $Pb(BO_2)_2$, as well as combinations thereof, can be used to achieve total evaporation of elements from any type of powdered sample [79].

X-Ray photoelectron spectroscopy (XPS, ESCA) is a surface quantitative spectroscopic technique that measures the chemical formula, chemical state, and electronic state of the elements that exist within a material. This technique uses monoenergetic soft X-rays which cause electrons to be ejected. Identification of the elements in the sample can be made directly from the kinetic energies of these ejected photoelectrons. Furthermore, the relative concentrations of elements can be determined from the photoelectron intensities. Other surface electron spectroscopy techniques include Auger electron spectroscopy (AES) and electron energy loss spectroscopy (EELS).

In order to study the chemical composition and chemical bonding situation in ceramic materials, resonance methods such as ESR, NMR and Mössbauer spectroscopy are used. For instance, *solid-state NMR spectroscopy* can be used for the microstructure analysis of silicon-containing amorphous polymer-derived ceramics (PDCs). By using ^{29}Si MAS NMR studies, it was found that polysilazane-derived Si–C–N ceramic materials showed only one amorphous Si–C–N phase, whereas polysilylcarbodiimide-derived PDCs consisted of amorphous Si_3N_4 nanodomains interconnected by amorphous carbon (for details, see Figure 1.10) [80].

The availability of tunable X-ray sources of a specific energy from synchrotrons allows *X-ray spectroscopy* to be used in a resonance mode that probes the excitation of core electrons of selected atoms instead of all the elements in the sample. As it reflects the electronic structure of unoccupied states of the selected element, this method is sensitive to the local environment of the selected atom. X-ray absorption spectra (XAS) show sharp absorption edges, followed by a decay curve which shows some fine structure called X-ray absorption fine structure (XAFS) [81]. The first 30 to 50 eV of XAFS correspond to X-ray absorption near edge structures (XANES), whereas the remainder of the spectrum is referred to as extended XAFS (EXAFS). Both XANES and EXAFS are sensitive to the local environment of the atoms and provide complementary information. Whereas XANES is sensitive to the chemical environment of the specific element, such as chemical bonding, charge state, magnetic state, EXAFS provides quantitative information about the local coordination of the atom such as coordination number and bond length. With reference to a standard and in combination with theoretical tools, XANES and EXAFS can serve as a powerful tool when analyzing small amounts of elements in various samples, such as ultra-thin films and ultra-dilute dopants [81].

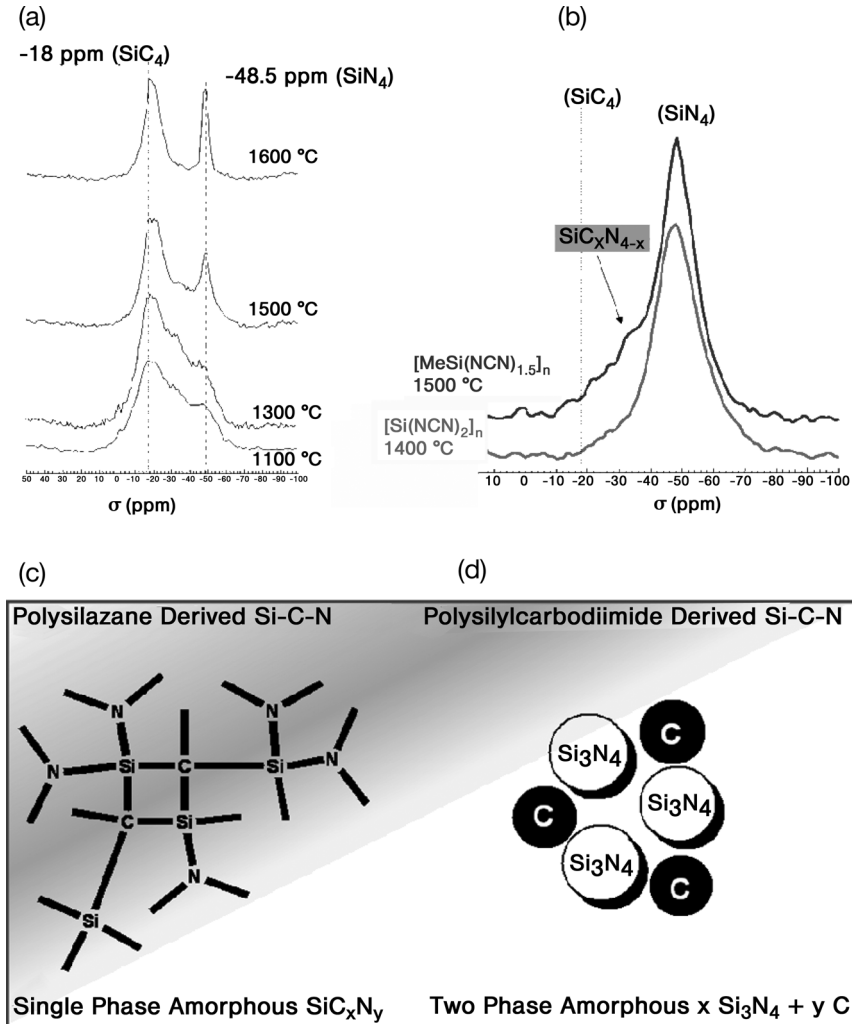


Figure 1.10 Solid-state NMR study of amorphous materials in the SiCN system. (a) ^{29}Si -MAS-NMR spectra of polysilazane-derived amorphous SiCN ceramic annealed at the given temperatures. (b) ^{29}Si -MAS-NMR spectra of poly(silylcarbodiimide)-derived amorphous SiCN ceramic annealed at 1400 and 1500 °C. While in (a) two chemical shift values are clearly developed at -18 ppm and -48.5 ppm indi-

cating the presence of SiC_4 and SiN_4 tetrahedra, the spectra of the poly(silylcarbodiimide)-derived SiCN ceramic exhibit only the resonance corresponding to SiN_4 moieties. The presence of the small shoulders at -34 and -21 ppm in the spectrum of the material annealed at 1500 °C indicates that the formation of mixed $\text{SiC}_x\text{N}_{4-x}$ tetrahedra ($x = 1-3$) starts at this temperature.

The electron energy loss near edge structure (ELNES) corresponds to the low-energy domain of electron energy loss spectrum (EELS) [82]. When measured in the transmission geometry, ELNES furnishes information which is almost identical to that provided by XANES. The ELNES/XANES technique has found applications in

the identification of polymorphs (GaN, AlN, InN, and ZnO) [83], the characterization of superficial and interfacial thin films [84], the identification of ultra-dilute dopants or impurities [85], solving the atomic structure of solid solutions, or in describing diluted magnetic semiconductors, such as ZnO:Mn polycrystalline materials [86].

In order to extract statistically representative information on the microstructure of advanced ceramics, such as void volume fraction, void size distribution, internal surface areas, pore morphologies, *small-angle scattering* (SAS) has been shown to be a good characterization method that complements other techniques such as X-ray microtomography or electron microscopy [87]. The quantitative parameters obtained from small-angle X-ray scattering (SAXS) or small-angle neutron scattering (SANS) complement the visual information obtained by scanning electron microscopy (SEM) and TEM or X-ray microtomography (XMT), the phase composition information as obtained by X-ray diffraction (XRD) and neutron diffraction (ND), and information obtained from other methods, from NMR to light scattering [87]. In particular, SAS methods (SAXS and SANS) provide information over macroscopic sample volumes, whereas electron microscopy only provides more local information for a small volume. Thus, SAS methods have found applications in the characterization of structural, electronic ceramics and glasses, in describing sintering, cavitation and damage processes, in quantifying microstructures with high interface densities, as well as in diagnostic studies of nanostructured, fractal materials and suspensions [87].

Transmission electron microscopy is a versatile electron optical technique to characterize microstructures, and has been used intensively for advanced ceramics in order to understand their properties, including grain boundary and interface phenomena [88]. For example, the TEM image shown in Figure 1.11 reveals the typical microstructure of a $\text{Si}_3\text{N}_4/\text{SiC}$ micro/nano-composite obtained by liquid-phase sintering of an amorphous SiCN powder. The image shows clearly that nano-sized SiC crystallites are embedded within micron-sized silicon nitride crystals, though some

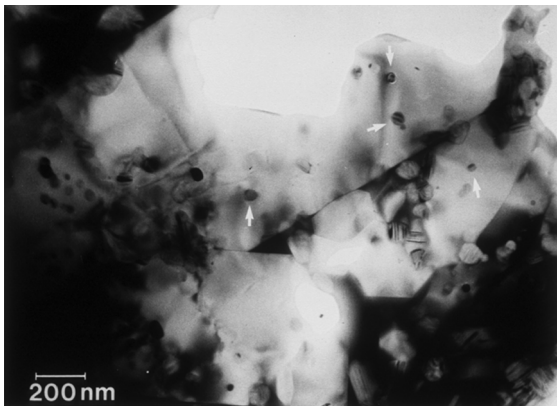


Figure 1.11 Transmission electron microscopy image of a $\text{Si}_3\text{N}_4/\text{SiC}$ micro/nano composite obtained by liquid-phase sintering of amorphous polysilazane-derived SiCN powder. The arrows indicate nanosized SiC crystallites. (Illustration courtesy R. Riedel.)

SiC is also found in the intergranular region. According to the design concept of structural ceramics developed by Niihara, this type of microstructure is denoted as an intra/inter-type nanocomposite [89]. In extensive studies, Niihara found that nanocomposites exhibited significantly enhanced mechanical properties.

The resolution of conventional high-resolution electron microscopy (HREM) is 0.17 to 0.20 nm at 200 to 300 kV, thus making the discrimination of atoms which are located closer than this distance impossible. Better resolutions of approximately 0.1 nm can be achieved with high-voltage atomic resolution electron microscopy (HVAREM). Using this technique, it is possible to discriminate light atoms, for example Ga and N, in GaN thin films [90]. A combination of HREM techniques, using methods such as nano-electron diffraction, energy dispersive X-ray spectroscopy (EDX) and electron holography, makes it possible to clarify atomic rearrangement, composition and electronic state structure of the nano-regions in advanced ceramics [91].

Although ceramics are hard, wear-resistant materials that retain a good degree of their mechanical properties even at high temperatures, they are very brittle and are unable to deform plastically under mechanical stress. For example, while hard metals may have a fracture toughness of up to $20 \text{ MPa m}^{-1/2}$, most advanced ceramics have toughness below $10 \text{ MPa m}^{-1/2}$ [92]. The failure of ceramic materials is dominated by fracture originating from sources of stress concentration – that is, their mechanical performances are dominated by the presence of processing defects (such as porosity, impurities, and microcracking) as much as by the microstructure [93].

There are several aspects of the microstructure which should be taken into account when describing the *mechanical features* of ceramic materials. The first is the physical nature of the features, such as the composition and crystal structure of the solid phases, and the presence of pores, microcracks, and impurity phases. The second aspect involves the microstructural scale of the features, such as their size, size distribution, volume fraction, and microstructural homogeneity. The third aspect is the orientation of microstructural features (e.g., morphological and crystallographic anisotropy) [93]. Thus, the challenge is to design materials with a phase and microstructure that delivers both high hardness and fracture toughness.

The *fracture toughness* in ceramics can be improved by various *extrinsic* shielding mechanisms, such as *in-situ* toughening (growth of platelets or whiskers within the microstructure), transformation toughening (transformation of tetragonal zirconia grains into the lower density monoclinic phase at the crack tip, thus generating crack closure forces), crack deflection, crack bridging (filament or fiber toughening), or microcrack toughening [94].

Hardness is defined as resistance to penetration [95], thus relating to a response of the surface to a mechanical load. Therefore, hardness is not necessarily a bulk property, and should be differentiated from *strength* [93]. There are typically two standard methods for measuring the hardness of ceramics, namely the Knoop and Vickers techniques. These involve the application of a load via a geometrically defined indenter, such as a steel ball (as in the Rockwell technique), a diamond square pyramid (Vickers), or an elongated diamond pyramid (Knoop). Although there is a well-known dependency of hardness on load, a full characterization by

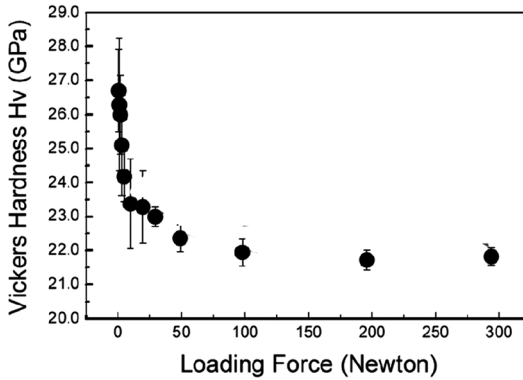


Figure 1.12 Hardness versus load relationship of a SiC-based ceramic, showing the strong dependence of the measured hardness of the applied load expressing the difficulties to determine a reliable hardness value [135].

hardness–load relationships is rather uncommon for ceramics (Figure 1.12). Furthermore, there is no relationship for converting different hardness test values (such as Knoop to Vickers hardness), thus making the hardness comparison of different ceramic materials difficult. Studies on the Vickers hardness of several brittle ceramics show hardness–load curves which exhibit a distinct transition to a plateau of constant hardness level; this involves a relationship between hardness (H), Young’s modulus (E), and fracture toughness (K_{IC}). Using these parameters, a “brittleness index” B was proposed that is derived from deformation and fracture energy ratios ($B \equiv HE/K_{IC}^2$) and was claimed to have a potential predictive value in ceramic design applications [92].

Besides toughness and hardness, there are several mechanical properties of ceramic materials which are relevant to their applications, including *wear resistance*, *hot hardness*, *creep resistance*, *tribochemical stability*, and *thermal expansion coefficient*.

Due to the thermal activation of additional deformation mechanisms (cross-slip of dislocations, creep via grain boundary and lattice diffusion, or viscous flow) the hardness decreases when materials are subjected to high temperatures. Symmetry of the crystal structure has dramatic effects on the *hot hardness* of the materials: for example, cubic boron nitride shows at ca. 600 °C only 50% of its original hardness, while the hardness of diamond decreases remarkably at about 1100 °C. Materials with less-symmetric crystal structures have fewer easy slip directions for thermally activated dislocation, thus featuring higher hot hardness values (e.g., B_4C , which is the hardest material known at temperatures around 1000 °C) [96].

The *thermal expansion coefficient* is a critical thermomechanical property of advanced ceramic materials, when either a composite, a material joint or a coating on a substrate is exposed to large changes in temperature. Thus, a misfit between the thermal expansion coefficients of the materials may cause cracking and delamination. For this reason, materials with low expansion coefficients are usually preferred, typically for cutting applications.

1.5

Applications of Advanced Ceramics

During the past few decades, advanced ceramics have been used for industrial applications due to their unique mechanical, thermal, chemical, electrical, magnetic, optoelectronic, superconducting and gas-sensing properties. As such, ceramics have become important for advanced technologies such as energy transformation, storage and supply, information technology, transportation systems, medical technology and manufacture technology. Several examples are given below.

When used as *cutting* and *slitting tools*, advanced ceramics may show many advantages over metal and conventional tungsten carbide tools, since they are hard, inert, non-metallic, and non-magnetic, retain their properties at high temperatures, and have longer lifetimes. Today, advanced ceramics find widespread use in machining and finishing applications. Ceramics used for cutting tools include alumina–silicon carbide whisker composites, silicon nitride, titanium carbide/titanium nitride materials (cermets), SiALONs, alumina–titanium carbide composites, polycrystalline diamond and cubic boron nitride [97].

Advanced ceramics are also very attractive for *electronic applications* as they can operate at high power and high frequencies, at high temperatures, and in harsh environments, and also combine properties such as electrical insulation and magnetism which is not possible for metals. Using chemically synthesized powders, materials such as oxides, nitrides, carbides, and borides have been fabricated with tailored microstructures and properties (including band gap, electron or hole charge carrier mobility) for electronic applications.

A recent example of newly synthesized materials explored for semiconductor and electro-optic applications is binary nitrides with spinel (Si_3N_4 , Ge_3N_4) and thorium phosphate (Zr_3N_4 , Hf_3N_4) structures. Besides high hardness, the novel nitride polymorphs of Si_3N_4 and Ge_3N_4 possess a direct band gap between 3.0 and 4 eV, which is comparable to the UV/blue light-emitting diode materials based on Al, Ga and In nitride [98,99]. The first such silicon nitride (cubic $\gamma\text{-Si}_3\text{N}_4$) was synthesized under a high pressure [100]. Other cubic spinel nitrides since studied [101,102] showed that many M_3N_4 ($\text{M}=\text{C}, \text{Si}, \text{Ge}, \text{Sn}, \text{Ti}, \text{Zr}$) and $c\text{-AB}_2\text{N}_4$ ($\text{A}=\text{C}, \text{Si}, \text{Ge}, \text{Sn}, \text{Ti}, \text{Zr}, \text{Hf}$; $\text{B}=\text{C}, \text{Si}, \text{Ge}, \text{Sn}, \text{Ti}, \text{Zr}, \text{Hf}$) compounds may also have interesting properties.

Another example of emerging ceramic semiconductors is that of silicon carbide. This material has excellent mechanical properties, oxidation resistance and corrosion resistance at high temperatures, and a band-gap (3.2 eV) which is three times as wide as that of silicon. This allows the application of SiC in semiconductor devices used in power electronics. A high electron velocity and a low intrinsic carrier concentration are other interesting properties of SiC. Various bulk growth methods for SiC single crystals have been developed during the past few years to facilitate these new applications [103].

Among insulators, one area where very rapid growth has been witnessed for ceramics is that of *microwave applications*. Temperature-stable, medium-permittivity dielectric ceramics have been used for decades as resonators in filters for microwave communication due to their very low dielectric loss (high-quality factor) and their

high permittivity. Thus, ceramic materials with simple and complex perovskite structures such as $(\text{Mg,Ca})\text{TiO}_3$, ZrTiO_4 , BaTi_4O_9 , $\text{BaZn}_{1/3}\text{Ta}_{2/3}\text{O}_3$ (BZT), $\text{CaTiO}_3\text{-NdAlO}_3$ (CTNA), $\text{ZrTiO}_4\text{-ZnNb}_2\text{O}_6$ (ZTZN), $\text{Ba}(\text{Co,Zn})_{1/3}\text{Nb}_{2/3}\text{O}_3$ (BCZN) are used for base station resonators, whilst $\text{Ba}_4\text{Nd}_{9,33}\text{Ti}_{18}\text{O}_{54}$ -based compounds find application as receivers in digital televisions [104].

Piezoceramics are materials which couple electrical and mechanical stimuli/responses. For example, when a mechanical force is applied, an electrical response arises which, in terms of voltage or charge, is proportional to the magnitude of the applied stress. Conversely, when an electric field is applied, a mechanical stress or deformation/shape change develops. Ceramics are widely used for electromechanical sensors and actuators. Some examples of piezo materials are crystalline quartz, barium titanate, vanadium niobate and lead zirconate titanate (PZT). Some of these piezomaterials, such as quartz, are single crystals which are not polarized in the stress-free state and whose piezoelectricity depends only on the crystal orientation. Other piezoelectrics, such as PZT, contain domains of spontaneous polarizations of different orientations [105]. Since the domains in the as-prepared materials are randomly oriented, a poling process is required in order to achieve domain alignment that gives rise to net piezoelectricity. This process is usually performed under a high electric field (ca. 10 kV cm^{-1}) at slightly elevated temperatures (ca. 100°C) for a short time.

During recent years, polymer-derived ceramics (PDCs) have been demonstrated as being new materials suitable for *micro electromechanical system (MEMS) applications*, especially at relatively high temperatures. MEMS is a device that often involves transduction processes which couple mechanical, electrical, thermal, magnetic, radiant, and chemical processes [106]. For instance, SiCO ceramics have been used in the preparation of MEMS by using mixtures of polysiloxane polymers with a variety of active (Ti, TiH_2 , Al) or passive (SiC, Al_2O_3 , TiB_2) fillers. Under micro molding, these polymers melt, are then solidified by chemical or thermal cross-linking, and the shaped green body is subsequently pyrolyzed to the final MEMS component. In this way, SiCO micro gear components [107,108] and a SiCON [109] micro igniter (Figure 1.13) have recently been developed using the polymer-to-ceramic transformation process.

Advanced ceramics are also increasingly used as materials for prostheses, such as *orthopedic* and *dental implants*, due to their good combination of stability, biocompatibility, strength, and wear resistance [110]. For example, leucite-reinforced glass ceramics have been used for dental implants (crowns), showing fracture strengths of 95 MPa [111] compared to porcelains that have fracture strength values of ca. 70 MPa. Zirconia (typically a solid solution with 3 mol.% Y_2O_3 to stabilize the tetragonal form) is also used commercially for this purpose. Tetragonal zirconia and alumina have been used as femoral heads in total hip replacements; zirconia (in the tetragonal form) has better strength and toughness, but alumina has a better thermal conductivity. Recently, alumina–zirconia nanocomposites were also explored for joint prostheses. The materials were synthesized by a new colloidal processing route which involves a stable suspension of high-purity alumina in diluted solutions of zirconium alkoxide. Due to the small size of zirconia nanograins and the narrow grain-size distribution thereof,

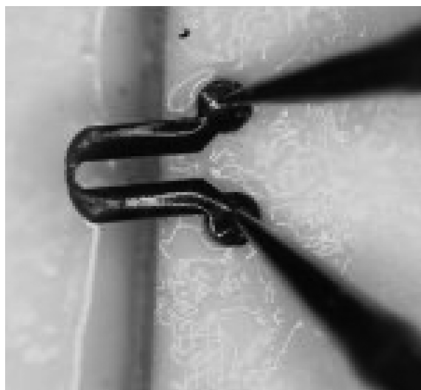


Figure 1.13 A micro igniter based on SiCON and produced from a pre-ceramic polymer. (Source: Rishi Raj, University of Colorado at Boulder.)

larger amounts of tetragonal zirconia could be retained in the material, thus contributing to improved fracture toughness ($5.9 \text{ MPa m}^{-1/2}$ for 10 vol.% ZrO_2). These nanocomposites can function at loads which are two-fold higher than the monoliths (ZrO_2 or Al_2O_3), without delayed fracture. Additionally, they show similar hardness values to alumina and are not susceptible to the hydrothermal instability observed in case of zirconia bioceramics [112].

Solid oxide fuel cells (SOFCs) utilize the rapid ionic conductivity of either oxygen or proton to allow solid-state charge transport across an oxide (electrolyte) membrane that separates oxidation and reduction reactions on two sides, consuming oxygen and fuel (H_2 or hydrocarbons). SOFCs offer the potential for efficient power generation in distributed power systems and transport systems, resulting in lower CO_2 emission and reduced pollution from combustion products such as NO_x and SO_x . SOFCs have some advantages over other types of fuel cell, for example their high operation temperatures allow the flexibility in the type of fuel that can be used [113]. Standard SOFCs operate at temperatures of about $900\text{--}1000^\circ\text{C}$, and use yttria-stabilized zirconia (YSZ, in the cubic form) as electrolyte. These high temperatures, however, generate considerable constraints on the materials that can be used for interconnections and balance of plant (e.g., LaCrO_3 degrades during long-term operation). Thus, some recent developments focus on new electrolytes (such as $\text{Ce}(\text{Gd})\text{O}_{2-x}$ or $\text{La}(\text{Sr})\text{GaO}_3$) that can maintain a sufficiently high ionic conductivity at lower operating temperatures of about 800°C . A lower operating temperature may also allow the application of other cell concepts which, along with improved fabrication processes, may have a significant potential for reducing the fabrication costs of SOFCs [114].

Chemical sensing is another application where the ionic or electronic conductivity of oxide ceramics is utilized. As the world becomes more environmentally and security conscious, chemical sensors are increasingly used in a wide range of industrial and consumer applications, such as steelmaking, metal casting, power

plants, airplanes, automobiles, and public safety. Many of these applications demand rugged and reliable sensors capable of operation in harsh environments. Chemical sensors detect the presence of various gases (CO , NO_x , O_2 , CO_2 , hydrocarbons, and volatile organic compounds) for emission control and air quality monitoring, as well as early warning of smoke, fire, and hazardous chemicals in public places and mass transportation systems [115]. One oxygen sensor, which is used in every vehicle for emission and combustion control, utilizes the same above-mentioned YSZ for SOFCs. In this application, a galvanic signal develops across the YSZ electrolyte to correspond to the partial pressure of oxygen in the exhaust gas. Many gas sensors use semiconductor metal oxide-based ceramic materials. These remain stable in air at high temperatures while reacting with gases (some of them are chemically aggressive) at their surfaces, without undergoing irreversible chemical reactions, as would other semiconductors (e.g., Si) [116]. These sensors may be broadly classified depending on how they utilize the various interaction mechanisms at the sensor surface: bulk conduction-based sensors (TiO_2 , BaTiO_3 , CeO_2 , Nb_2O_5), metal/oxide junction controlled sensors (Pd/SnO_2 , Pt/TiO_2), and surface-layer conductive sensors. For example, SnO_2 -based bulk-type sensors integrated with a direct or an indirect heating coil (Ir–Pd or Cr alloy wire) operating at temperatures of 300–450 °C are widely used for toxic and inflammable gas leak detectors [116]. In addition to YSZ and SnO_2 , perovskite-type oxides (ABO_3) are well represented in sensor applications due to their ability to exhibit a wide range of ionic and electronic conduction behaviors. For example, LnFeO_3 -based ($\text{Ln}=\text{La}$, Sm) sensors have shown good sensitivity to CO and NO_2 [117], and $\text{SmFe}_{1-x}\text{Co}_x\text{O}_3$ -based sensors have shown good response and recovery behavior to O_3 and NO_2 [117]. Another ceramic of interest is for In_2O_3 -based sensors; with different dopants (Ga, P, B, Se, Bi, Cu, and Mn), this material shows different selectivity for different gases [118].

During the past two decades, much research effort has been expended concerning the development and manufacture of ceramic materials for *thermal barrier coatings* (TBCs) on turbine parts. TBCs are used to coat transition pieces, combustion lines, first stage blades and vanes and other hot-path components of gas turbines, as well as in aerospace applications [119]. TBC materials must respect certain basic requirements such as a high melting point, no phase transformation in the temperature range from room temperature to the operating temperature, chemical inertness, low thermal conductivity, thermal expansion match with the substrate, good adherence to the substrate, and low sintering rate of the porous microstructure [120]. Thus, very few ceramic materials have been used as TBCs, such as zirconia, stabilized zirconia materials (3YSZ, 7-8YSZ, 18YSZ, 5 wt.% $\text{CaO} + \text{ZrO}_2$), mullite, alumina, ceria, LaZr_2O_7 , GdZr_2O_7 , BaZrO_3 , titania, $\text{Y}_3\text{Al}_5\text{O}_{12}$ (YAG), $\text{LaMgAl}_{11}\text{O}_{19}$, LaPO_4 , NiCo-CrAlY (bond coat of TBC) or superalloys (e.g., IN737 as substrate of TBC) [119]. The most frequently used compounds are zirconia-based materials, partially or fully stabilized by magnesia or other alkaline-earth metal oxides (calcia, strontia, barium oxide), yttria, hafnia, ceria or other rare-earth metal oxides (REO), such as gadolinia, neodymia, dysprosia, lanthana, or other transition metal oxides (e.g., nickel oxide, iron oxide, cobalt oxide, scandium oxide), to yield a zirconia tetragonal microstructure that resists phase changes. Due to the high-temperature stability, low thermal

conductivity, and relatively simple deposition by plasma spraying, flame spraying or PDV techniques, YSZ materials have been extensively used for TBC applications. Nevertheless, these materials have some disadvantages, such as the limited operation temperature for long-term applications (<1473 K, above which temperature sintering occurs), phase transformation (above 1443 K) which leads to the formation of cracks in the coating [121], and the presence of a high concentration of oxygen ion vacancies which, at high temperature, assist the oxygen transport and oxidation of the bond coat at the ceramic–bond coat interface (the formation of thermally grown oxide, TGO) [122].

Silicon-based ceramics and ceramic matrix composites (CMCs) show great promise as candidates for high-temperature structural components in next-generation gas turbine engines. However, they show a rapid degradation in a water vapor atmosphere, due to volatilization of the protective silica scale. Thus, the normally protective silica scale [123], which is responsible for the excellent oxidation resistance of the silicon-containing ceramics in clean, dry oxygen, can be severely degraded by reacting with impurities such as alkali salts [124] or water vapors [125]. The most promising approach to enhance the protection of these materials from water vapor attack is the use of plasma-sprayed external *environmental barrier coatings* (EBCs) [126]. One of the first systems to be considered as an EBC candidate for the protection of SiC was a double-layered mullite–zirconia-based system (a mullite layer on SiC followed by a top layer of zirconia) [125]. The advantages of the system lay in the close match of the coefficients of thermal expansion for SiC and mullite. Nevertheless, the expansion of the zirconia top layer was observed to be almost twice that of SiC, which caused cracking in the coating on thermal cycling, and eventual delamination [127]. The presence of cracks in the zirconia layer, which propagated into existing cracks in the mullite layer, led to the exposure of mullite, and resulted in silica loss from the mullite. Consequently, further cracking occurred in the mullite, and this resulted in SiC oxidation. Other materials were studied as EBC candidates in order to match the coefficient of thermal expansion and to guarantee phase stability, low volatility in the operating temperature range and the ability to act as a barrier to steam. Calcium aluminosilicate (CAS), yttrium silicate and barium strontium silicate were found to be suitable materials for EBCs [126]. Despite these materials showing certain disadvantages, such as the need for heat treatment after thermal spraying (in case of CAS), it was shown that these EBCs would provide protection to the CMC substrates, thereby achieving a three-fold improvement in their useful lifetime.

The development of *structural ceramics for high-temperature applications* has become an important topic during the past few decades. Ceramics must exhibit certain properties for high-temperature applications, such as oxidation resistance, chemical stability, low volatility, resistance to creep deformation at interfaces, sufficient toughness at ambient temperature, and thermal-shock resistance [128]. Studies on these properties showed that, in general, non-oxide ceramics (e.g., SiC, SiN) are promising for applications at high temperatures, but are unlikely to operate above 1500°C . While ceramic oxide/non-oxide composites may react at temperatures above 1200°C , oxide-based ceramics can be designed to have, for example, substantial creep resistance in the range of 1500 to 2000°C .



Figure 1.14 Ceramic matrix composite (CMC) for application as motor-cycle brakes. The CMC is produced from a carbon fiber fabric infiltrated by a SiC forming a pre-ceramic polymer. After the polymer infiltration process (PIP), the device is transformed into a C_f/SiC_m composite by high-temperature annealing. The Starblade™ brake disc promises an improved brake performance, together with an enhanced lifetime. (Source: Starfire Systems, Inc.)

In recent years, PDCs have been investigated for their use as structural ceramics in high-temperature applications such as ceramic brakes (Figure 1.14) [66]. Polymer-derived Si–C–N ceramics have been found to exhibit superplasticity and high strength and fracture toughness at elevated temperatures after *in-situ* crystallization to β - Si_3N_4/β -SiC composites [129]. In contrast, amorphous Si–C–N materials have been reported to have ultrahigh temperature creep and oxidation resistance. Decomposition was observed in nitrogen and nitrogen-free atmospheres above 1500–1600 °C, due to the presence of excess carbon in the materials compositions [130]. Polymer-derived silicoboron carbonitride materials (Si–B–C–N) have remarkably higher thermal, chemical, and mechanical stability than boron-free silicon carbonitrides. Their extraordinary thermal stability up to 2000 °C in a protective atmosphere is believed to rely on kinetic rather than thermodynamic reasons. Thus, structural disorder in the Si–B–C–N ceramics which results in increased free activation energies for crystallization and solid-state reaction of the Si–N bond with carbon provides the thermal stability for these materials [131]. Furthermore, the presence of β - Si_3N_4 , even at temperatures up to 2200 °C in nitrogen, indicates that carbon and boron kinetically stabilize the Si–B–C–N composition, thereby enforcing a stabilizing effect on Si_3N_4 [132].

Recently, it was shown that the presence of ZrO_2 in Si–C–N ceramic systems improves their oxidation resistance [133]. Furthermore, the presence of ZrO_2 (in the form of a zirconium alkoxide) in the polymeric precursor allowed the preparation of SiCN– ZrO_2 fibers by altering the rheological behavior of the pre-ceramic polymer [134]. As this functionalization method of SiCN precursors has been claimed to be

fairly general, alkoxides of metals such as titanium, hafnium, silicon and aluminum can be used for modifying the rheology of the polymers and preparing SiCN-based ceramic fibers.

1.6

Outlook

Despite the relatively small sales of less than US\$50 billion per year, advanced ceramic products form an integral part of modern technology that underlies the World's economy and human civilization. Most of these products work "behind the scene", as ceramic bearings in the pumps on an airplane, as catalyst supports in a catalytic converter in a truck, as oxygen sensors in an integrated steel mill, as a cold/hot water valve in a kitchen faucet, or as an insert and joint in a replaced hip. These advanced ceramic products are precise and long-lasting, requiring little maintenance yet performing crucial functions. They are also relatively new, becoming commonplace only during the past 20 years. However, during the next 20 years other advanced ceramic products – both small and large – will undoubtedly emerge, and some will surely play a crucial role in our future. For example, if commercially viable SOFCs using zirconia and dye-sensitized solar cells using anatase become available, they will help to meet the World's energy needs, with reduced pollution-related costs and a suppression of the greenhouse gas effect.

Where they are used, advanced ceramic products usually offer superior performance that cannot be replicated by other materials. Despite their intrinsic attributes, however, advanced ceramics almost always encounter high entry barriers – largely because material designers and engineers are not familiar with the properties and manufacture of ceramics, and so rarely specify a ceramic product in its own right. Nevertheless, when an advanced ceramic product is successfully introduced to the market place, over time it typically enjoys an increasing market share, and is seldom displaced by another material.

There is a common impression, shared among most ceramists, that advanced ceramic products are expensive to manufacture and difficult to mass produce, and hence are sold only to small markets not known for large profits. In reality, advanced ceramic products need not be expensive. For example, approximately 10^{12} multilayer ceramic capacitors (MLCC) are sold every year for about US\$10 billion for use in computers, televisions, cell phones and other consumer products. Thus, the manufacturing cost is about 1 US cent per piece, which contains hundreds of engineered thin layers of high-K dielectrics and electrodes. Advanced ceramic products can also be highly profitable. For example, among the components of a flat-screen television, the thin glass sheet that supports the liquid crystal display (LCD) has the highest profit margin.

Clearly, low-cost, high-profit margin, mass-produced advanced ceramic products are possible, and advanced ceramics do indeed have a bright future. The key to this success is a superior material/manufacturing technology and unique product attributes, coupled with entrepreneurship and business execution. On the technical side,

innovation and a better understanding of all aspects of advanced ceramics are evidently needed. These include the discovery of new ceramic compounds and forms, designs from first principles, detailed characterization of key processing steps and properties, and affordable manufacturing technology from start to finish for products with desired microstructure and properties. The subsequent chapters in this book, and in other volumes of this series, provide a more detailed view of some of these aspects.

References

- 1 Horvath-Bordon, E., Riedel, R., Zerr, A., McMillan, P.F., Auffermann, G., Prots, Y., Bronger, W., Kniep, R. and Kroll, P. (2006) *Chem. Soc. Rev.*, **35**, 987.
- 2 Zerr, A., Riedel, R., Sekine, T.I., Lowther, J.E., Ching, W.-Y. and Tanaka, I. (2006) *Adv. Mater.*, **18**, 2933.
- 3 Wu, X. and Chen, I.-W. (1992) *J. Am. Ceram. Soc.*, **75**, 1846.
- 4 Wakei, F. (2006) *J. Am. Ceram. Soc.*, **89**, 1471.
- 5 (a) Clark, D.E. and Sutton, W.H. (1996) *Annu. Rev. Mater. Sci.*, **26**, 299; (b) Katz, J.D., Blade, R.D. and Scherer, C.P. (1989) *Ceram. Eng. Sci. Proc.*, **19**, 857.
- 6 Glade, S.C. and Thadhani, N.N. (1995) *Met. Mater. Trans.*, **26**, 2565.
- 7 Dogan, C.P., Rawers, J.C., Govier, R.D. and Korth, G. (1994) *Nanostr. Mater.*, **4**, 631.
- 8 Nygren, M. and Shen, Z. (2003) *Solid State Sci.*, **5**, 125.
- 9 Shen, Z., Johnsson, M., Zhao, Z. and Nygren, M. (2002) *J. Am. Ceram. Soc.*, **85**, 1921.
- 10 (a) Grins, J., Ezmaeilzadeh, S. and Berastegui P. (2001) *J. Mater. Chem.*, **11**, 112358; (b) Shen, Z. and Nygren, M. (2001) *J. Eur. Ceram. Soc.*, **21**, 611.
- 11 Shen, Z. and Nygren, M. (2002) *Key Eng. Mater.*, **206–213**, 2155.
- 12 (a) Misra, R.S., Mukherjee, A.M. and Yamazaki, K. (1996) *J. Mater. Res.*, **11**, 1144; (b) Goodwin, T.J., Yoo, S.H., Matteazzi, P. and Groza, J.R. (1997) *Nanostr. Mater.*, **8**, 559; (c) Kimura, H. and Kobayashi, S. (1994) *J. Japan Inst. Met.*, **58**, 201; (d) Nishimura, T., Mitomo, M., Hirotsuru, H. and Kawahara, M. (1995) *J. Mater. Sci. Lett.*, **14**, 1046.
- 13 (a) Greiner, A. (1992) Diploma thesis, University of Stuttgart; (b) Lecomte, E. (1999) PhD thesis, Darmstadt University of Technology.
- 14 Jahanmir, S., Ramnlu, M. and Koshy, P. (eds) (1998) *Machining of Ceramics and Composites*, Marcel Dekker Inc, USA.
- 15 Marinescu, I.D., Tonshoff, H.K. and Inasaki, I. (eds) (1999) *Handbook of Ceramic Grinding and Polishing*, William Andrew Publishing, Norwich, NY, USA.
- 16 Wang, L. and Aldinger, F. (2002) *Adv. Eng. Mater.*, **2**, 110.
- 17 Mutsuddy, B.C. and Ford, R.G. (1995) *Ceramic Injection Molding*, Chapman & Hall, London.
- 18 Lange, F.F. and Luther, E.P. (1994) in: *Tailoring of Mechanical Properties of Si₃N₄ Ceramics*, (eds M.J. Hoffmann, and G. Petzow), Kluwer Academic, Dordrecht.
- 19 Graule, T.J., Gauckler, L.J. and Baader, F.H. (1996) *Ind. Ceram.*, **16**, 31.
- 20 Omatete, O.O., Janney, M.A. and Nunn, S.D. (1997) *J. Eur. Ceram. Soc.*, **17**, 407.
- 21 Kosmac, T., Novak, S. and Sajko, M. (1997) *J. Eur. Ceram. Soc.*, **17**, 427.
- 22 Griffin, E.A. and McMillin, S. (1995) *Ceramic Processing and Sintering*, Vol.6 Marcel Dekker, New York.

- 23 Stierlen, P. and Eyerer, P. (1999) (eds D. L. Bourell J.J. Beaman, R.H. Crawford, H.L. Marcus, and J.W. Barlow), Proceedings of the Solid Freeform Fabrication Symposium Austin, Texas.
- 24 Griffith, M.L. and Halloran, J.W. (1996) *J. Am. Ceram. Soc.*, **79**, 2601.
- 25 Agarwala, M.K., Bandyopadhyay, A., Weeren, R.W., Safari, A., Danforth, S. C., Langrana, N.A., Jamalabad, V.R. and Whalen, P.J. (1996) *Am. Ceram. Soc. Bull.*, **75**, 60.
- 26 Cima, M.J. and Sachs, E.M. (1991) *Ceramic Processing and Sintering*, Vol.2 Marcel Dekker, New York.
- 27 Teng, W.D. and Edirisinghe, M.J. (1998) *Br. Ceram. Trans. J.*, **97**, 169.
- 28 Sinton, D.P., Besman, T.M. and Loden, R.A. (1988) *Ceram. Bull.*, **67**, 350.
- 29 Kato, A., Hojo, J. and Watasi, T. (1982) *Mater. Sci. Res.*, **17**, 123.
- 30 Fitzer, E. and Hegen, D. (1979) *Angew. Chem.*, **91**, 316.
- 31 Riedel, R., Kunesch, J., Passing, G., Kaysser, W.A. and Petzow, G. (1990) (eds R.B. Bhagat, A.H. Clauer, P. Kumar, and A.M. Ritter), Proceedings International Conference on Metal and Ceramic Matrix Composites: Processing, Modelling and Mechanical Behaviour, TMS-Verlag, p. 579.
- 32 Riedel, R. and Gaudl, K. (1991) *J. Am. Ceram. Soc.*, **74**, 1331.
- 33 Zhou, Y., Probst, D., Thissen, A., Kroke, E., Riedel, R., Hauser, R., Hoche, H., Broszeit, E., Kroll, P. and Stafast, H. (2006) *J. Eur. Ceram. Soc.*, **26**, 1325.
- 34 Chase, M.W., Davis, C.A., Downley, J. R., Fridup, D.J., McDonald, R.A. and Syvernd, A.N. (1985) Janaf Thermochemical Tables. *J. Phys. Chem. Ref. Data*, 3rd edn, **14**.
- 35 Zelinski, B.J.J. and Uhlmann, D.R. (1984) *J. Phys. Chem. Solids* **45**, 1069.
- 36 Defay, R., Prigogine, I., Bellemans, A. and Everett, D.A. (1966) in *Surface Tension and Adsorption*, Longman, London.
- 37 Scherer, G.W. (1990) *J. Am. Ceram. Soc.*, **73**, 3.
- 38 Mazdiyansi, K.S., Dolloff, R.T. and Smith, J.S. (1969) *J. Am. Ceram. Soc.*, **52**, 523.
- 39 Brown, L.M. and Mazdiyansi, K.S. (1970) *Inorg. Chem.*, **9**, 2783.
- 40 (a) Farbenindustrie, I.G. (1925) Deutsches Patent, 475557. (b) *Chem. Abstr.*, (1929) **23**, 3718.
- 41 Augst, F. and Sufraga, F. (1971) *Deutsche Offen.*, 2033373.
- 42 Herman, D.F. (1953) US Patent 2654770. *Chem. Abstr.* 1954, **48**, 13710.
- 43 Bradley, D.C. and Wardlaw, W. (1950) *Nature*, **165**, 75.
- 44 Dislich, H. (1971) *Angew. Chem.*, **83**, 428.
- 45 Hench, L.L. (1984) *Mater. Res. Soc. Symp. Proc.*, **32**, 101.
- 46 Pflanz, K., Riedel, R. and Chmiel, H. (1992) *Adv. Mater.*, **4**, 662.
- 47 Kulig, M., Oroschin, W. and Greil, P. (1989) *J. Eur. Ceram. Soc.*, **5**, 209.
- 48 Roosen, A. and Bowen, H.K. (1989) (ed. H. Hausner), Proceedings 2nd International Conference on Ceramics and Powder Processing Science, Deutsche Keramische Gesellschaft, Bad Honnef.
- 49 Jenett, H., Bubert, H., Riedel, R. and Stadelmann, H. (1990) *Mikrochim. Acta [Wien]*, **II**, 207.
- 50 (a) Barringer, E.A. and Bowen, H.K. (1982) *J. Am. Ceram. Soc.*, **65**, C-199; (b) Matijevic, E. (1989) (ed H. Hausner), Proceedings 2nd International Conference on Ceramics and Powder Processing Science, Deutsche Keramische Gesellschaft, Bad Honnef.
- 51 Barringer, E.A. and Bowen, H.K. (1985) *Ceram. Eng. Sci. Proc.*, **5**, 285.
- 52 Schmidt, H. (1990) *Erzmetall*, **43**, 75.
- 53 Sakka, S. (1988) *J. Non-Cryst. Solids*, **100**, 142.
- 54 Dislich, H. (1988) (ed P. Picozzi), Proceedings of the European Meeting

- "Inorganic Coating on Glass", University of L'Aquila p 113.
- 55 Schmidt, H. (1989) *J. Non-Cryst. Solids*, **112**, 419.
- 56 Schubert, U., Breitscheid, B., Amberg-Schwab, S. and Buhler, H. (1990) *Small Metal Particles in Ceramic Matrices by Sol-Gel Processing of Metal Complexes*. Lecture 7th Cimtec World Ceramic Congress, Italy.
- 57 Schubert, U. (1991) *Kleine Metall- und Metalloxidpartikel in keramischen Matrices*. Lecture DFG-Kolloquium, "Schwerpunktprogramm Keramische Hochleistungswerkstoffe", Bonn.
- 58 Schmidt, H., Seiferling, B., Phillip, G. and Deichmann, K. (1988) (eds J.D. Mackenzie and D. Ulrich), *Ultrastructure Processing of Advanced Ceramics*, John Wiley, New York, p. 651.
- 59 Gabriel, A. and Riedel, R. (1997) *Angew. Chem.*, **109**, 371.
- 60 Kroke, E., Völger, K.-W., Klönczynski, A. and Riedel, R. (2001) *Angew. Chem. Int. Ed.*, **40**, 1698.
- 61 (a) Ainger, F.W. and Herbert, J.M. (1965) in: *Special Ceramics*, (ed P. Popper), Academic Press, New York, p 168; (b) Chantrell, P.G. and Popper, P. (1965) in: *Special Ceramics*, Academic Press, New York, p 76.
- 62 Fritz, G. (1956) *Z. Anorg. Allg. Chem.*, **286**, 149.
- 63 Yajima, S., Hayashi, J. and Imori, M. (1957) *Chem. Lett.*, **9**, 931.
- 64 (a) Verbeek, W. (1973) German Patent No. 2218960. (Bayer AG), (US Patent No. 3853567), November 8; (b) Verbeek, W. and Winter, G. (1974) German Patent No. 2236078 (Bayer AG) March 21; (c) Winter, G., Verbeek, W. and Mansmann, M. (1974) German Patent No. 2243527 May 16.
- 65 Yajima, S., Hasegawa, Y., Okamura, K. and Matsuzawa, I. (1978) *Nature (London)*, **273**, 525.
- 66 Riedel, R., Mera, G., Hauser, R. and Klönczynski, A. (2006) *J. Ceram. Soc. Jpn.*, **114**, 425.
- 67 Wilson, A.M., Zank, G., Eguchi, K., Xing, W., Yates, B. and Dahn, J.R. (1997) *Chem. Mater.*, **9**, 1601.
- 68 Dubrovnic, P.R. (1995) in: *Silicon Containing Polymers, The Royal Society of Chemistry, Cambridge*, p185.
- 69 (a) Soraru, G.D., D'Andrea, G., Campostrini, R., Babonneau, F. and Marriotto, G. (1995) *J. Am. Ceram. Soc.*, **78**, 379; (b) Trassl, S., Motz, G., Rössler, E. and Ziegler, G. (2002) *J. Am. Ceram. Soc.*, **85**, 239; (c) Trassl, S., Kleebe, H.-J., Störner, H., Motz, G., Rössler, E. and Ziegler, G. (2002) *J. Am. Ceram. Soc.*, **85**, 1268; (d) Belor, V., Corriu, R.J.P., Leclercq, D., Mutin, P.H. and Vioux, A. (1992) *J. Polym. Sci.*, **30**, 613.
- 70 Klönczynski, A., Schneider, G., Riedel, R. and Theissmann, R. (2004) *Adv. Eng. Mater.*, **6**, 64.
- 71 Kroke, E., Li, Y.-L., Konetschny, C., Lecomte, E., Fasel, C. and Riedel, R. (2000) Review article: Silazane-derived ceramics and related materials. *Mater. Sci. Eng.*, **R26**, 97.
- 72 Iwamoto, Y., Völger, W., Kroke, E. and Riedel, R. (2001) *J. Am. Ceram. Soc.*, **84**, 2170.
- 73 Riedel, R., Kienzle, A., Dressler, W., Ruwisch, L., Bill, J. and Aldinger, F. (1996) *Nature*, **382**, 796.
- 74 Pump, J. and Rochow, E.G. (1964) *Z. Anorg. Allg. Chem.*, **330**, 101.
- 75 Riedel, R., Greiner, A., Miehe, G., Dressler, W., Fuess, H., Bill, J. and Aldinger, F. (1997) *Angew. Chem. Int. Ed. Engl.*, **36**, 603.
- 76 (a) Gabriel, A.O., Riedel, R., Strock, S. and Maier, W. (1997) *Appl. Organomet. Chem.*, **11**, 833; (b) Riedel, R., Kroke, E., Greiner, A., Gabriel, A.O., Ruwisch, L., Nicolich, J. and Kroll, P. (1998) *Chem. Mater.*, **10**, 2964.
- 77 Miller, R.D. and Michl, J. (1989) *Chem. Rev.*, **89**, 1359.

- 78 West, R. and Carberry, R. (1975) *Science*, **189**, 179.
- 79 Nickel, H. and Zadgorska, Z. (1993) *Spectrochim. Acta*, **488**, 25.
- 80 Iwamoto, Y., Völger, W., Kroke, E. and Riedel, R. (2001) *J. Am. Ceram. Soc.*, **84**, 2170.
- 81 Tanaka, I., Mizoguchi, T. and Yamamoto, T. (2005) *J. Am. Ceram. Soc.*, **88**, 2013.
- 82 Egerton, R.F. (1996) *Electron Energy-Loss Spectroscopy in the Electron Microscope*, Plenum Press, New York.
- 83 Mizoguchi, T., Tanaka, I., Yoshioka, S., Kunisu, M., Yamamoto, T. and Ching, W.Y. (2004) *Phys. Rev. B*, **70**, 045103.
- 84 Kimoto, K., Matsui, Y., Nabatame, T., Yasuda, T., Mizoguchi, T., Tanaka, I. and Toriumi, A. (2003) *Appl. Phys. Lett.*, **83**, 4306.
- 85 (a) Tanaka, I., Mizoguchi, T., Matsui, M., Yoshioka, S., Adachi, H., Yamamoto, T., Okajima, T., Umesaki, M., Ching, W.Y., Inoue, Y., Mizuno, M., Araki, H. and Shirai, Y. (2003) *Nature Mater.*, **2**, 541; (b) Mizoguchi, T., Sakurai, M., Nakamura, A., Matsunaga, K., Tanaka, I., Yamamoto, T. and Ikuhara, Y. (2004) *Phys. Rev. B*, **70**, 153101.
- 86 Kunisu, M., Oba, F., Ikeno, H., Tanaka, I. and Yamamoto, T. (2005) *Appl. Phys. Lett.*, **86**, 121902.
- 87 Allen, A.J. (2005) *J. Am. Ceram. Soc.*, **88**, 1367.
- 88 Ikuhara, Y. (2002) *J. Ceram. Soc. Jpn.*, **110**, 139.
- 89 Niihara, K. (1991) *J. Ceram. Soc. Jpn.*, **99**, 974.
- 90 Iwamoto, C., Shen, X.Q., Okumura, H., Matsuhata, H. and Ikuhara, Y. (2001) *Appl. Phys. Lett.*, **79**, 3941.
- 91 Oku, T. (2001) *J. Ceram. Soc. Jpn.*, **109**, S17.
- 92 Quinn, J.B. and Quinn, G.D. (1997) *J. Mater. Sci.*, **32**, 4331.
- 93 Sherman, D. and Brandon, D. (1999) *Adv. Eng. Mater.*, **1**, 161.
- 94 Ritchie, R.O. (1999) *Int. J. Fracture*, **100**, 55.
- 95 McCole, I.J. (1990) *Ceramic Hardness*, Plenum, New York.
- 96 Swain, M.V. (1994) (eds R.W. Cahn, P. Haasen, and E.J. Kramer), *Materials Science and Technology*, Vol.11 VCH, New York.
- 97 Whitney, E.D. (1994) *Ceramic Cutting Tools*, Noyes Publications, New Jersey.
- 98 Nakamura, S. (1997) *MRS Bull.*, **22**, 29.
- 99 Ponce, F.A. and Bour, D.P. (1997) *Nature*, **386**, 351.
- 100 Zerr, A., Miede, G., Serghiou, G., Schwarz, M., Kroke, E., Riedel, R., Fuess, H., Kroll, P. and Boehler, R. (1999) *Nature*, **6742**, 340.
- 101 Ching, W.-Y., Mo, S.-D., Ouyang, L., Rulis, P., Tanaka, I. and Yoshiya, M. (2002) *J. Am. Ceram. Soc.*, **85**, 75.
- 102 Oba, F., Tatsumi, K., Tanaka, I. and Adachi, H. (2002) *J. Am. Ceram. Soc.*, **85**, 97.
- 103 Sudarshan, T.S. and Maximenko, S.I. (2006) *Microelectron. Eng.*, **83**, 155.
- 104 Reaney, J.M. and Iddles, D. (2006) *J. Am. Ceram. Soc.*, **87**, 2063.
- 105 (a) Kamlah, M. (2001) *Continuum Mech. Thermodyn.*, **13**, 219; (b) Kamlah, M. and Wang, Z. (2003) *Computational Mater. Sci.*, **28**, 409.
- 106 Korvink, J.G. and Paul, O. (2006) *MEMS*, William Andrew Publishing, Springer, Norwich, NY, USA.
- 107 Harshe, R., Balan, C. and Riedel, R. (2004) *J. Eur. Ceram. Soc.*, **24**, 3471.
- 108 Harshe, R. (2004) Ph. D. Thesis, TU Darmstadt.
- 109 Liew, L.-A. (2002) Ph. D. Thesis, University of Colorado at Boulder.
- 110 Rekow, D. and Thompson, V.P. (2007) *J. Mater. Sci: Mater. Med.*, **18**, 47.
- 111 Guazzato, M., Albakry, M., Ringer, S.P. and Swain, M.V. (2004) *Dent. Mater.*, **20**, 441.
- 112 Chevalier, J., De Aza, A.H., Fantozzi, G., Schehl, M. and Torrecillas, R. (2000) *Adv. Mater.*, **12**, 1619.

- 113 Metcalfe, I.S. (2003) *Chem. Eng. Technol.*, **26**, 857.
- 114 Holtappels, P., Vogt, U. and Graule, T. (2005) *Adv. Eng. Mater.*, **7**, 292.
- 115 Szabo, N., Lee, C., Trimboli, J., Figueroa, O., Ramamoorthy, R., Midlam-Mohler, S., Soliman, A., Verweij, H., Dutta, P. and Akbar, S. (2003) *J. Mater. Sci.*, **38**, 4239.
- 116 Park, C.O. and Akbar, S.A. (2003) *J. Mater. Sci.*, **38**, 4611.
- 117 Itagaki, Y., Mori, M., Hosoya, Y., Aono, H. and Sadaoka, Y. (2007) *Sensors and Actuators B*, **122**, 315.
- 118 Korotcenkov, G., Boris, I., Cornet, A., Rodriguez, J., Cirera, A., Golovanov, V., Lychkovsky, Yu. and Karkotsky, G. (2007) *Sensors and Actuators B*, **120**, 657.
- 119 Cao, X.Q., Vassen, R. and Stoever, D. (2004) *J. Eur. Ceram. Soc.*, **24**, 1.
- 120 (a) Cernuschi, F., Bianchi, P., Leoni, M. and Scardi, P. (1999) *J. Therm. Spray Technol.*, **8**, 102; (b) Vassen, R., Tietz, F., Kerkoff, G., Stoever, D., Lecomte-Beckers, J. and Schuber, F. (1998) (ed J. Ennis) Proceedings of the 6th Liege Conference on Materials for Advanced Power Engineering, Forschungszentrum Jülich GmbH, Jülich, Deutschland, p. 1627.
- 121 Thornton J. and Majumdar, A. (1995) (ed A. Ohmori), Proceedings of the 14th International Thermal Spray Conference. Thermal Spray: Current Status and Future Trends, ASM International, Kobe, Japan, p. 1075.
- 122 Vassen, R., Kerkhoff, G. and Stoever, D. (2001) *Mater. Sci. Eng. A*, **303**, 100.
- 123 Jacobson, N.S. (1993) *J. Am. Ceram. Soc.*, **76**, 3.
- 124 Jacobson, N.S., Smialek, J.L. and Fox, D.S. (1990) in: *Handbook of Ceramics and Composites*, (ed N.S. Cheremisinoff), Marcel Dekker, New York, p 99.
- 125 Opila, E.J. and Hann, R. (1997) *J. Am. Ceram. Soc.*, **80**, 197.
- 126 Lee, K.N. (2000) *Surface Coatings Technol.*, **133–134**, 1.
- 127 Eaton, H.E. and Linsey, G.D. (2002) *J. Eur. Ceram. Soc.*, **22**, 2741.
- 128 Raj, R. (1993) *J. Am. Ceram. Soc.*, **76**, 2147.
- 129 Wakai, F., Komada, Y., Sakaguchi, S., Murayama, M., Izaki, K. and Niihara, K. (1990) *Nature (London)*, **344**, 421.
- 130 (a) Riedel, R., Passing, G., Schönefelder, H. and Brook, R.J. (1992) *Nature (London)*, **355**, 714; (b) Riedel, R., Kleebe, H.-J., Schönefelder, H. and Aldinger, F. (1995) *Nature (London)*, **391**, 773.
- 131 Wang, Z.-C., Aldinger, F. and Riedel, R. (2001) *J. Am. Ceram. Soc.*, **84**, 2179.
- 132 (a) Matsunaga, K., Iwamoto, Y., Fischer, C.A.J. and Matsubara, H. (1999) *J. Ceram. Soc. Jpn.*, **107**, 1025; (b) Matsunaga, K. and Iwamoto, Y. (2001) *J. Am. Ceram. Soc.*, **84**, 2213.
- 133 Saha, A., Shah, S.R. and Raj, R. (2004) *J. Am. Ceram. Soc.*, **87**, 1556.
- 134 Saha, A., Shah, S.R. and Raj, R. (2003) *J. Am. Ceram. Soc.*, **86**, 1443.
- 135 Brazhkin, V., Dubrovinskaia, N., Nicol, M., Norikov, N., Riedel, R., Soloshenko, V. and Zhao, Y. (2004) *Nature Materials*, **3**, 576.